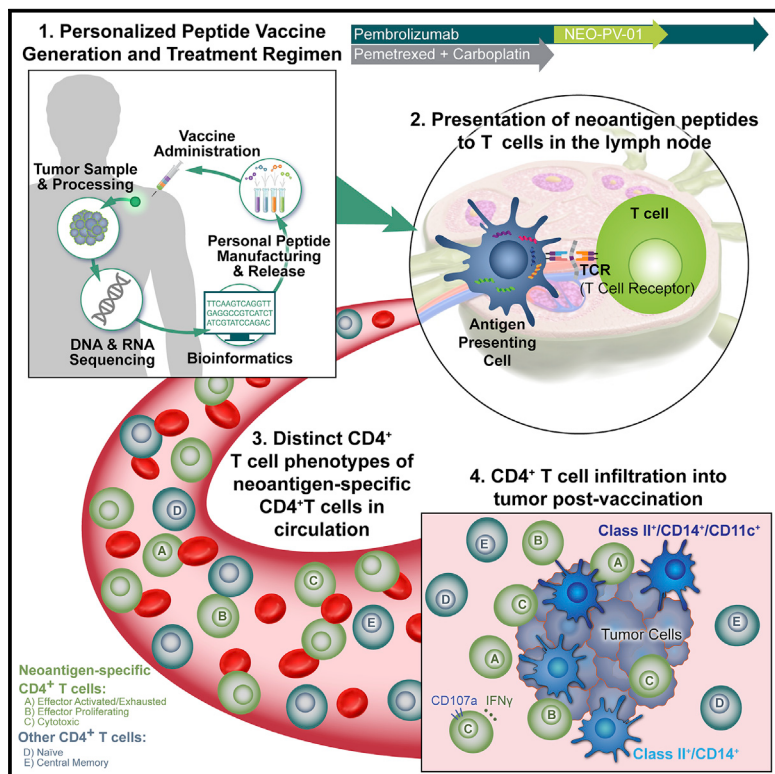


Personalized neoantigen vaccine NEO-PV-01 with chemotherapy and anti-PD-1 as first-line treatment for non-squamous non-small cell lung cancer

Graphical abstract



Authors

Mark M. Awad, Ramaswamy Govindan, Kristen N. Balogh, ..., Mark DeMario, Richard B. Gaynor, Lakshmi Srinivasan

Correspondence

richard.gaynor@biontech.us (R.B.G.), lakshmi.srinivasan1@external.biontech.us (L.S.)

In brief

In a Phase Ib clinical study, Awad et al. demonstrate feasibility, safety, and immunogenicity of NEO-PV-01 plus chemotherapy and PD-1 inhibition in advanced NSCLC as a first-line treatment. Neoantigen-specific CD4⁺ T cells have an activated effector phenotype. CD4⁺ T cells infiltrate tumors post-vaccination and induce epitope spread to other neoantigens such as mutant KRAS.

Highlights

- NEO-PV-01 plus chemotherapy and anti-PD-1 is feasible and safe in first-line NSCLC
- Regimen generates durable and cytotoxic neoantigen-specific T cell responses
- Neoantigen-specific CD4⁺ T cells have an activated effector phenotype
- Vaccine-induced T cells induce epitope spread to mutant KRAS epitopes



Article

Personalized neoantigen vaccine NEO-PV-01 with chemotherapy and anti-PD-1 as first-line treatment for non-squamous non-small cell lung cancer

Mark M. Awad,¹ Ramaswamy Govindan,² Kristen N. Balogh,³ David R. Spigel,⁴ Edward B. Garon,⁵ Meghan E. Bushway,³ Asaf Poran,³ Joong Hyuk Sheen,³ Victoria Kohler,³ Ekaterina Esaulova,³ John Srouji,³ Suchitra Ramesh,³ Rohit Vyasamneni,³ Binisha Karki,⁵ Tracey E. Sciuto,³ Himanshu Sethi,⁶ Jesse Z. Dong,³ Melissa A. Moles,³ Kelledy Manson,³ Michael S. Rooney,³ Zakaria S. Khondker,³ Mark DeMario,³ Richard B. Gaynor,^{3,*} and Lakshmi Srinivasan^{3,7,*}

¹Dana Farber Cancer Institute, Brigham and Women's Hospital, Harvard Medical School, Boston, MA, USA

²Washington University School of Medicine, St. Louis, MO, USA

³BioNTech US, Cambridge, MA, USA

⁴Tennessee Oncology, Nashville, TN, USA

⁵David Geffen School of Medicine, University of California, Los Angeles, Los Angeles, CA, USA

⁶Natera, Austin, TX, USA

⁷Lead contact

*Correspondence: richard.gaynor@biontech.us (R.B.G.), lakshmi.srinivasan1@external.biontech.us (L.S.)

<https://doi.org/10.1016/j.ccel.2022.08.003>

SUMMARY

Neoantigens arising from mutations in tumor DNA provide targets for immune-based therapy. Here, we report the clinical and immune data from a Phase Ib clinical trial of a personalized neoantigen-vaccine NEO-PV-01 in combination with pemetrexed, carboplatin, and pembrolizumab as first-line therapy for advanced non-squamous non-small cell lung cancer (NSCLC). This analysis of 38 patients treated with the regimen demonstrated no treatment-related serious adverse events. Multiple parameters including baseline tumor immune infiltration and on-treatment circulating tumor DNA levels were highly correlated with clinical response. *De novo* neoantigen-specific CD4⁺ and CD8⁺ T cell responses were observed post-vaccination. Epitope spread to non-vaccinating neoantigens, including responses to KRAS G12C and G12V mutations, were detected post-vaccination. Neoantigen-specific CD4⁺ T cells generated post-vaccination revealed effector and cytotoxic phenotypes with increased CD4⁺ T cell infiltration in the post-vaccine tumor biopsy. Collectively, these data support the safety and immunogenicity of this regimen in advanced non-squamous NSCLC.

INTRODUCTION

It has been recognized increasingly that somatic mutations in tumor cells can lead to the presentation of neoantigens, which can be recognized by the host immune system and directly lead to tumor cell killing (Ott et al., 2017; Keskin et al., 2019; Hu et al., 2021). Numerous clinical trials have attempted to harness this mechanism of inducing tumor control by using personalized neoantigen-based vaccination, particularly in the setting of solid tumors with a high neoantigen load, with some promising data, especially in the adjuvant setting (Ott et al., 2017; Sahin et al., 2017; Keskin et al., 2019; Hilf et al., 2019). Studies have shown that a high neoantigen burden is associated with favorable clinical responses and increased progression-free survival (PFS) in patients with solid tumors, including non-small cell lung cancer (NSCLC) treated with anti-programmed cell death protein 1 (PD-1) (Rizvi et al., 2015; Luksza et al., 2017; Hellmann et al., 2018).

We have previously reported on a similar personalized neoantigen-based vaccine trial in combination with anti-PD-1 in patients with advanced melanoma, NSCLC, and transitional cell carcinoma (TCC) of the bladder. In this study, patients were treated with a personalized peptide vaccine of up to 20 unique peptides (NEO-PV-01) targeted toward high-quality neoepitopes identified using a bioinformatics algorithm as described previously (Ott et al., 2020). The study demonstrated the safety and feasibility of this therapy, as well as the ability to deeply characterize the immune responses generated against the vaccine peptides (Ott et al., 2020).

Immune checkpoint inhibitors targeting PD-1 or PD-L1 are well established as a first-line standard of care for NSCLC, both in combination with cytotoxic chemotherapy regimens or as monotherapy (Gandhi et al., 2018; Reck et al., 2019; Borghaei et al., 2020; Awad et al., 2021; Rodríguez-Abreu et al., 2021). A dual checkpoint inhibitor regimen targeting PD-1 and CTLA-4



has also demonstrated improved outcomes over chemotherapy and is an additional approved first-line treatment (Hellmann et al., 2019; Paz-Ares et al., 2021). Despite these major advances, there is still a need for additional options to further extend survival in this patient population. The addition of a neoantigen vaccine to a regimen of chemotherapy and pembrolizumab presents an opportunity to induce and expand tumor-specific immune responses.

We report here data from a Phase Ib clinical trial combining NEO-PV-01, pemetrexed, carboplatin, and pembrolizumab in first-line metastatic non-squamous NSCLC (NCT03380871). In addition to demonstrating that this treatment regimen was safe and well tolerated, we performed detailed molecular and immune analyses of both the tumor microenvironment (TME) and peripheral blood from these patients. The analyses presented here suggest a robust effect of peptide vaccination in combination with chemotherapy and anti-PD-1, particularly on CD4⁺ T cells, supporting further investigation of this treatment in additional clinical trials.

RESULTS

Treatment with NEO-PV-01 plus chemotherapy and anti-PD-1 is feasible and safe in first-line non-squamous NSCLC

The study was designed as a single-arm study to assess the safety and immunogenicity of NEO-PV-01 in combination with chemotherapy and pembrolizumab in first-line non-squamous NSCLC. Patients were enrolled at four clinical sites in the United States. The protocol specified no prior systemic treatment for metastatic disease and no prior immunotherapy with anti-PD-1 or PD-ligand 1 (PD-L1) antibodies. Tumor PD-L1 status was assessed for all of the patients, but enrollment was not restricted based on PD-L1 status ([STAR Methods](#)). The primary objective of this Phase Ib trial was to evaluate the safety of administering NEO-PV-01 with pembrolizumab/chemotherapy; secondary objectives included determination of antitumor activity such as objective response rate (ORR), PFS, and overall survival (OS). In addition, exploratory endpoints included a comprehensive immune analysis in blood and tumor ([STAR Methods](#); [Data S1](#)).

Production of NEO-PV-01 was performed as previously described (Ott et al., 2020). Briefly, tumor mutations were first identified by whole-exome and RNA sequencing of each patient's formalin-fixed tumor and matched normal cells from blood as outlined in the vaccine manufacturing schema ([Figure 1A](#)). Epitopes were then selected based on bioinformatic algorithms as previously described in Ott et al. (2020) and incorporated into peptide-based neoantigen vaccines (Nielsen and Andreatta 2016; Abelin et al., 2017). Each neoantigen vaccine consisted of up to 20 unique peptides that were formulated in up to 4 distinct pools with adjuvant poly-ICLC (polyinosinic-polycytidylic acid stabilized with polylysine and carboxymethylcellulose). Patients received a combination of pembrolizumab, pemetrexed, and carboplatin administered every 3 weeks (a cycle) for four cycles during vaccine production. Pemetrexed maintenance therapy was not administered in this study. Following this initial triplet therapy, starting at week 12, NEO-PV-01 was administered intramuscularly in four separate anatomical locations. As reported previously (Ott et al., 2020), five priming and two booster doses

of NEO-PV-01 were given over a period of the next 12 weeks. Pembrolizumab was continued both during the vaccine and post-vaccine time periods up to 2 years in the absence of unacceptable toxicities or disease progression ([Figure 1B](#)).

Between May 2018 and April 2019, 38 patients were enrolled and received at least one dose of pembrolizumab and were defined as the intention-to-treat (ITT) set ([Figure 1C](#)). Among these patients, 3 (8%) had prior therapy, with 2 of the 3 patients receiving cisplatin plus pemetrexed for 3 months as an adjuvant regimen. The third patient had 3 prior therapies that included carboplatin plus paclitaxel for 3 months, followed by erlotinib for 2 years, and a vaccine therapy (α 1,3 galactosyltransferase) for 4 months as adjuvant regimens. Most of the patients (87%) in our study presented with stage IV disease ([Table 1](#)). Seventeen of the 38 patients (45%) in the ITT set were not vaccinated due to early study termination for reasons including the inability to manufacture vaccine due to inadequate tumor and/or sufficient number of neoantigens (10 patients), adverse events (2 patients), patient consent withdrawn (2 patients), progressive disease, an investigator decision, or administration of a study-prohibited concomitant medication (1 patient each). Therefore, the vaccinated patient subset (VAX) included 21 patients, of which 16 completed vaccination (full VAX), with five discontinuing treatment due to progressive disease during the vaccine regimen ([Figure 1C](#)). Analysis of the mutational status for common mutations observed in NSCLC among the ITT patient set of 38 patients revealed 19 patients with KRAS mutations, 15 patients with TP53 mutations, 6 patients with KEAP1 mutations, and no STK11 mutations ([Table S1](#)). Depending on the patient's human leukocyte antigen (HLA) alleles and predicted binding affinity of the driver mutants, these common mutations were either included as part of the vaccine or were monitored for epitope spread analysis ([Table S1](#)). A TP53 and a KEAP1 mutation were included in the vaccine for the corresponding patients. The reasons that driver mutations were not included in the vaccine or monitored for epitope spread were either very low immunogenicity scores as defined by our prediction pipeline or the predicted immunogenic peptides had poor solubility and failed the manufacturing process.

The primary objective of the study was to evaluate the safety and tolerability of NEO-PV-01 in combination with pembrolizumab, pemetrexed, and carboplatin ([Table S2](#)). The regimen was well tolerated, consistent with the pembrolizumab plus pemetrexed/carboplatin safety profile. The most frequent related adverse events (AEs) included nausea, emesis, diarrhea, fatigue, neutropenia, and anemia. The only related AE with clear increased incidence in the VAX group were injection site reactions, with 6 patients (29%) experiencing transient, low-grade events. Treatment-related serious adverse events (SAEs) were uncommon, reported in 5 patients, only 1 of whom was in the VAX group (<5%). Treatment discontinuations due to related AEs were also uncommon (2 patients, 5.3%), and no grade 5 events were observed. In summary, NEO-PV-01 in combination with pembrolizumab, pemetrexed, and carboplatin was safe and well tolerated, with a safety profile similar to that previously reported in metastatic NSCLC (Ott et al., 2020).

ORR (RECIST version 1.1, patients who achieve complete response [CR] or partial response [PR], clinical benefit rate [CBR, patients who achieve CR, PR or stable disease [SD]],

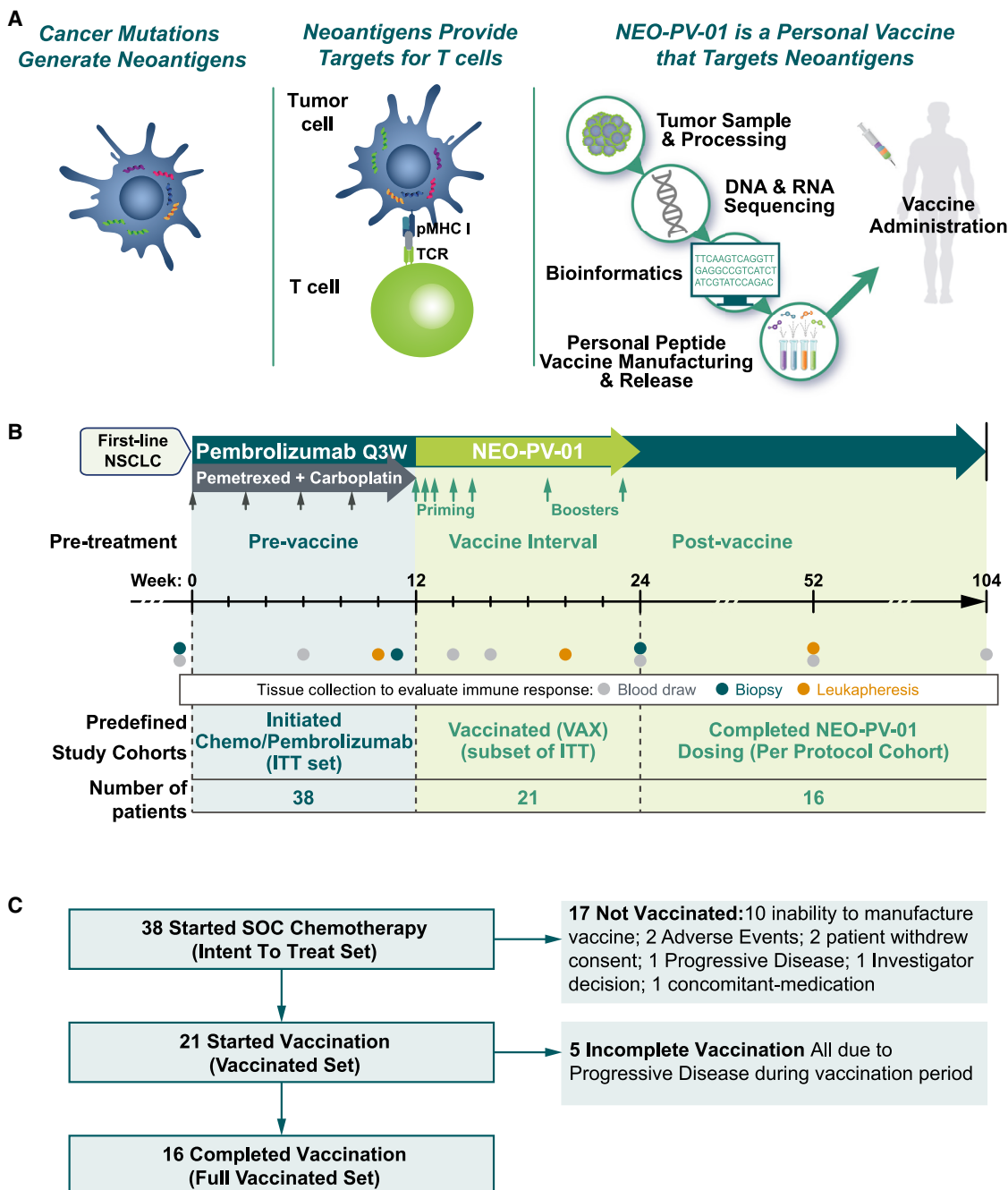


Figure 1. NEO-PV-01 vaccine generation, clinical study design, and patient disposition

(A) Schematic for sequencing of patients' tumors, prediction of neoantigens restricted to MHC class I molecules, and generation of the synthetic long peptides included in the personalized neoantigen vaccines (tumor cell in blue, T cell in green).

(B) Treatment scheme. Treatment with pembrolizumab and pemetrexed plus carboplatin was initiated at week 0; NEO-PV-01 was then administered between weeks 12 and 24, with pembrolizumab continuing for up to 2 years.

(C) Study patient disposition. Seventeen of the 38 patients (45%) in the ITT set were not vaccinated due to early study termination for reasons including inability to manufacture vaccine due to inadequate tumor and/or insufficient number of neoantigens (10 patients), adverse events (2 patients), patient consent withdrawn (2 patients), progressive disease, an investigator decision, or administration of a study-prohibited concomitant medication (1 patient each). See also Tables S1 and S2.

PFS and OS were analyzed with a minimum follow-up of 24 months as of the August 2021 data cutoff. Figures 2A and 2B summarize the radiographic response profiles for each pa-

tient (change in sum of target lesions) for the VAX set and a subset of the ITT set, respectively. Only patients with at least one post-baseline RECIST assessment are shown in Figure 2B.

Table 1. Patient demographics and baseline disease characteristics

| | ITT (N = 38) | VAX (N = 21) |
|--|-----------------|----------------|
| Median age, y | 62.5 (56–73) | 63 (56–69) |
| Sex, M/F, n (%) | 15 (39)/23 (61) | 7 (33)/14 (67) |
| Prior therapy, n (%) | 3 (8%) | 0% |
| Stage IV, n (%) | 33 (87) | 21 (100) |
| Median TMB (range) ^a | 141 (2–776) | 279 (96–776) |
| Smokers (current or prior), % | 82 | 95 |
| Tumor PD-L1 expression, n (%) ^b | | |
| <1% | 11 (42) | 9 (43) |
| ≥1% – < 50% | 12 (46) | 10 (47) |
| ≥50% | 3 (12) | 2 (10) |
| Median sum of target lesions, cm | 8.6 | 8.3 |
| ECOG 0/1, n (%) | 11 (29)/27 (71) | 7 (33)/14 (67) |

^aTMB is represented as count of non-silent mutations detected in exonic regions.

^bTumor PD-L1 expression NA for 12 of 38 ITT patients.

The pair of nested bar plots (Figure 2A) for the vaccinated patients allows for the comparison of the best response before vaccine initiation (darker shade) and the best response overall (lighter shade). The difference indicates a further reduction in tumor size following the initiation of vaccine. Among the 21 patients who received at least one dose of NEO-PV-01, two patients had a further decrease in the sum of target lesion size of more than 30% post-vaccination (Figure 2A). A Swimmer's plot for all of the patients in the ITT set provides detailed information on treatment schedules for each patient, as well as time of progression, and indicates any case in which a patient achieved a post-vaccination reduction of tumor size by at least 30% (Figure 2C).

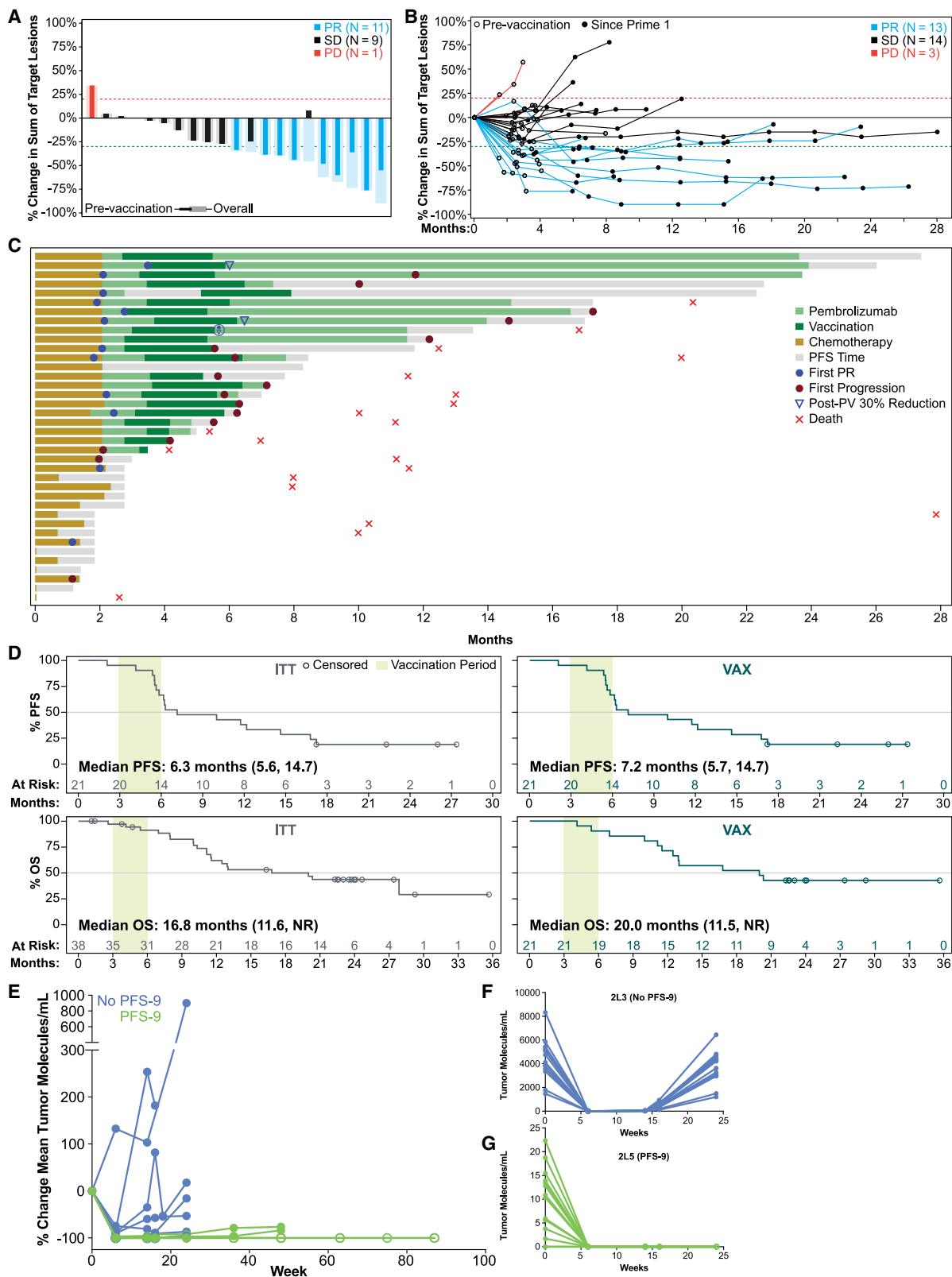
The ORR/CBR (with 95% confidence interval [CI]) for the ITT and VAX sets were 34%/71% (19.6–51.4/54.1–84.6) and 69%/100% (41.3–89.0/79.4–100), respectively. Kaplan-Meier estimates for PFS and OS in both the ITT and VAX cohorts are shown in Figure 2D. Median PFS (95% CI) for ITT patients was 6.3 months (5.6–14.7) and for VAX patients was 7.2 months (5.7–14.7). Median OS for ITT patients was 16.8 months and for VAX patients was 20 months (11.6, NR ITT set, 11.5, NR VAX group). Tumor PD-L1 status for patients in the VAX group is shown in Figure S1A. Consistent with checkpoint therapy (Hellmann et al., 2018), patients with higher tumor PD-L1 staining had better clinical outcomes. Among the VAX set of 21 patients, 4 of 5 patients (80%) who progressed during vaccination phase and 5 of 16 patients (31.25%) who completed vaccination (full VAX set) had no PD-L1 expression on tumor cells at the pre-treatment time point.

Levels of circulating tumor DNA (ctDNA) in the peripheral blood plasma have been shown to be indicative of overall tumor burden and to predict relapse and response in multiple solid tumor indications (Abbosh et al., 2017; Corcoran and Chabner 2018; Snyder et al. 2019). In this study, two personalized and tu-

mor-informed ctDNA assays (Powles et al., 2021) were designed and tested for each patient to measure the levels of ctDNA. Of these 32 variants, 16 were predicted to be high-quality neoepitopes based on our internal bioinformatics algorithms previously described by Ott et al. (2020) (Figure S1B). The other set of 16 variants may not have been included in the vaccination, depending on the overlap between the Natera and our variant algorithm selection output, but they were shown to be tumor specific (Figure S1C). For this post hoc analysis, we used an exploratory endpoint defined by lack of progression at 9 months (PFS-9) post-initiation of treatment with pembrolizumab and chemotherapy. A median PFS of 8.8 months was observed previously with pembrolizumab plus chemotherapy in first-line metastatic non-squamous NSCLC patients (Gandhi et al., 2018). Overall, the mean neoantigen change of all variants tested per patient remained undetectable for patients who achieved PFS-9 (9 patients), while the majority of patients who did not achieve PFS-9 (no PFS-9, 8 patients) showed stable or increasing amounts of neoantigen-specific ctDNA molecules (Figure 2E). Figure 2F provides an example of the data at the individual neoantigen level for a patient who did not achieve PFS-9 (2L3), and Figure 2G provides an example of a patient who did achieve PFS-9 (2L5). Interestingly, the overall pattern of change in ctDNA levels is consistent across all mutations measured for these two patients, suggesting that no one neoantigen is able to escape under conditions of tumor control, and in the case of progressive disease, all of the previously detected neoantigens are present during a period of tumor regrowth.

Correlates with clinical response are observed pre-treatment in the TME, including T cell infiltration, major histocompatibility complex (MHC) class II expression, and T cell receptor (TCR) diversity

It has been shown previously that the infiltration of T and B cells into the tumor correlates with responses to checkpoint therapy (Helmink et al., 2020; Petitprez et al., 2020; Cabrita et al., 2020). We also observed multiple immune infiltrate readouts to correlate with clinical responses in our study. First, we observed that infiltration of both CD4⁺ and CD8⁺ T cells into the TME at the pre-treatment time point correlates with clinical response, suggesting that the immune state of the tumor before the patient undergoes treatment can predict response to the treatment regimen (Figure 3A). Analysis of the specific localization of CD4⁺ and CD8⁺ T cells revealed that infiltration of CD4⁺ T cells into areas with tumor cells correlates positively with response, whereas the localization of CD8⁺ T cells outside of the tumor areas correlates positively with response (Figure 3A). An example of a patient who achieved PFS-9 (2L5) and a patient who did not achieve PFS-9 (2L3) is shown in Figure 3B. Second, we observed that HLA class II gene expression in the tumor biopsies at the pre-treatment time point correlates positively with clinical outcome (Figure 3C). This is further supported by analysis for MHC class II expression at the protein level by multiplex immunofluorescence. We observed strong MHC class II staining (HLA-DR) specifically in cells of the monocyte lineage (CD14, CD11c) in the TME for patient 2L5 who achieved PFS-9 when compared to a patient who did not achieve PFS-9 (2L3) (Figure 3D). MHC class II expression by cells of the monocytic lineage in the TME suggest the presence of monocyte-derived



(legend on next page)

dendritic cells (DCs) and macrophages that may provide targets for neoantigen-specific CD4⁺ T cells, leading to better tumor control for patients with high expression of MHC II. The TCR repertoire in the pre-treatment TME was also assessed both by calculating the normalized Shannon's entropy (Jia et al., 2015; Hanson et al., 2020), as well as overall complementarity determining region (CDR3) unique amino acid (aa) sequences. This analysis revealed a positive correlation between PFS and TCR diversity (Figure 3E). We were also able to monitor the changes in TCR diversity over time in a smaller subset of post-treatment tumor biopsies. We observed an overall pattern toward increased or stable diversity during the course of the study for patients who achieved PFS-9, while those who did not achieve PFS-9 generally show decreasing TCR diversity over the course of the study (Figure 3F).

NEO-PV-01 plus chemotherapy and anti-PD-1 induces neoantigen-reactive T cell responses that are neo-epitope specific, persistent, and show cytotoxic potential

The overall immunogenicity of NEO-PV-01 plus chemotherapy and anti-PD-1 was assessed in patients' peripheral blood by measuring interferon γ (IFN- γ) secretion in response to recall with the vaccinating peptides. In total, T cell responses were assessed for 204 vaccinating peptides across 13 patients with available samples. Consistent with our previous report (Ott et al., 2020), the percentage of vaccine peptides generating an immune response in this assay was minimal at the pre-vaccine time point and increased across all 13 patients assessed at the post-vaccine time point (8 weeks after the first dose of vaccine) (Figures 4A and S2A). We observed an average of 55% of vaccine epitopes generating any T cell response using this assay (Figure 4B). Of these responses, 49% were detectable *ex vivo* in an overnight assay with added peptide, and the remaining responses were seen after a 5-day stimulation with added peptide. Overall, 100% of patients elicited at least one measurable response *ex vivo* (Figure 4B). A total of 94% of the immune responses to the vaccine peptides were seen only in the post-vaccination time point.

The percentage of epitopes generating either a CD4⁺ or CD8⁺ T cell response for each patient was measured across the 13 patients analyzed, resulting in 39% of epitopes generating a CD4⁺ T cell responses, while 31% generated CD8⁺ T cell responses (Figure 4B). The specificity of these immune responses to the neo-epitope as compared to the wild-type epitope was also tested across a range of peptide concentrations. Stronger reactivity to the neo-epitope was observed in 18 of 19 epitopes

tested (95%) across 5 patients (Figure 4C; Table S3). These data are consistent with the specificity of the immune response for neoantigens as previously reported (Ott et al., 2017, 2020; Hu et al., 2021).

Persistence of the vaccine-induced immune responses was also assessed for a subset of patients at 52 weeks after initiating the study (29 weeks after the final dose of vaccine). Of the 34 epitopes tested at week 52, 85.3% still had a response present at this late time point (Figures 4D and S2B). We also observed responses at week 52 that were not present at the week 20 post-vaccination time point for patients 2L13 (IM14), 2L14 (IM25), and 2L16 (IM23), indicating the potential for delayed generation of vaccine-induced responses (Figure S2B, green). A preexisting immune response was also observed for p53 R213L (IM14) neoantigen in patient 2L16 that was also observed at the week 52 time point (Figure S2B). These data suggest that overall, the immune responses generated in this study persisted for up to at least 1 year.

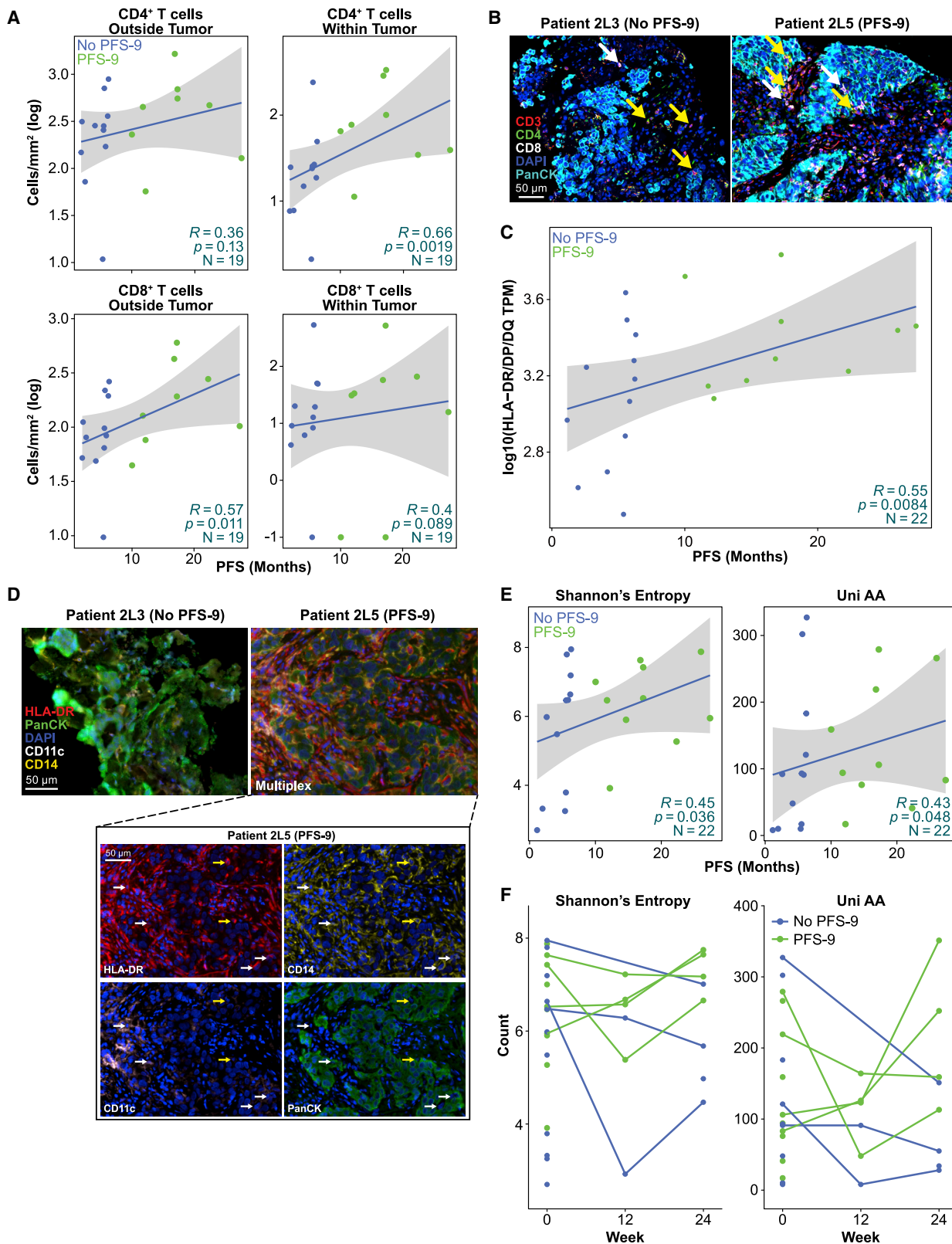
The cytotoxic potential of the T cell responses generated against the vaccinating peptides was assessed by measuring the level of co-expression of IFN- γ and CD107a (a marker of degranulation and cytotoxic potential; Betts et al., 2003) expression on CD4⁺ and CD8⁺ T cells, when assayed in the presence of neoantigen peptide (Figure 4E). In total, 92 vaccinating peptides were tested across 12 patients. Co-expression of IFN- γ and CD107a was observed for 56 of the 92 (61%) peptides tested, with 11 of 12 patients showing at least one cytotoxic response (92%) (Figures 4F, S3A, and S3B). Interestingly, when each cytotoxic response was characterized as either a CD4⁺ or CD8⁺ T cell response based on the subset of T cells that showed increased co-expression when compared to the DMSO-treated control cells, 93% of responses were characterized solely as CD4⁺ responses, and the remaining 7% showed a response in both the CD4⁺ and CD8⁺ compartments (Figure 4F).

NEO-PV-01 plus chemotherapy and anti-PD-1 induces epitope spread responses in most patients analyzed, with mutant KRAS responses observed in multiple patients

Given the cytotoxic phenotype of many of the T cell responses against the neoantigen vaccine epitopes, we speculated that tumor cell killing by these T cells could reveal additional epitopes, boosting the overall immune response to the patients' tumor. This concept, known as epitope spread, has been reported in a number of studies assessing T cell responses to vaccines (Corbiere et al., 2011; Kreiter et al., 2015; Ott et al., 2020; Hu et al., 2021). To quantitate epitope spread in this study, we analyzed

Figure 2. Rates and durability of responses following treatment with NEO-PV-01 plus chemotherapy and anti-PD-1

- (A) Best radiographic change (%) in sum of target lesions for each patient who received at least 1 dose of vaccine (VAX set). The dark-shaded narrow bars represent the best change pre-NEO-PV-01; the light-shaded wider bars represent the best overall change for patients who received at least 1 dose of NEO-PV-01 plus anti-PD-1. Red indicates progressive disease, gray indicates stable disease, and blue indicates partial response.
 - (B) Radiographic changes (%) in target lesions after initiation of pembrolizumab treatment for each patient (colors are the same as in A). Included are 30 of 38 ITT patients who had at least 1 post-baseline RECIST assessment.
 - (C) Swimmer's plot summarizing all of the patients in study. Each bar represents 1 subject in the study; bar length represents time on study.
 - (D) Kaplan-Meier estimates of PFS (top) and OS (bottom) for both the ITT (left) and vaccinated (right) patient sets.
 - (E–G) Measurement of ctDNA in the peripheral blood of a subset of patients as measured by the percent change in mean tumor molecules per milliliter of blood; open circles represent non-detectable levels of ctDNA. (E) Example of quantification of individual mutant ctDNA molecules detected in a no-PFS-9 patient (F) and a PFS-9 patient (G).
- See also Figure S1.



(legend on next page)

additional circulating T cell responses to highly ranked neoepitopes that were not included in the vaccine (referred to as “non-immunizing peptides,” or “NIMs”). Immune responses that were detected only at the post-vaccine time point (week 20) were considered to be epitope spread responses. Across 13 patients analyzed, 9 patients (69%) demonstrated epitope spread (Figures 5A and 5B). Of note were the epitope spread responses that were seen to the driver mutations. Of 19 patients who harbored KRAS mutations in the study, immune responses were measured for 7 of them. Three patients had an epitope spread response to G12C and one patient had a response to a G12V epitope (Figure 5C; Table S1). Of the 4 patients who had epitope spread to a KRAS mutation, 3 of them achieved PFS-9 on the study. The three patients whose epitope spread to mutant KRAS was not observed harbored the mutations G12V, G12C, and G12A respectively. Stronger reactivity to the neo-epitope when compared to wild type was demonstrated in all 4 patients in whom an epitope spread response to a KRAS mutant epitope was observed (Figure 5D). We additionally assessed the cytotoxic potential of these epitope spread responses by measuring co-expression of IFN- γ and CD107a as in Figure 4E. Of the 26 NIMs tested, 11 (42%) were cytotoxic, with 3 of 8 patients showing at least 1 cytotoxic response (38%). All of the cytotoxic responses observed were CD4 $^{+}$ responses, further supporting the importance of antitumor CD4 $^{+}$ responses in this study (Figures S4A and S4B). Interestingly, the KRAS G12C specific CD4 $^{+}$ response (NIM101) from patient 2L15 showed cytotoxic potential in this assay (Figure 5E). The presence of KRAS mutations in our study was positively associated with improved PFS (Figure S4C), suggesting the immunogenicity to KRAS mutations may in part be driving better clinical outcomes with our treatment regimen. Persistence of these epitope spread responses was also assessed at the week 52 time point for three patients with available samples (Figures S4D and S4E). Of the 10 epitopes tested, 80% were also detected at this later time point, consistent with the observation made to the vaccinating epitopes in Figure 4D. For patient 2L16, an additional epitope spread response (NIM12) was observed at week 52 that was not detectable at week 20, suggesting that epitope spread to additional antigens may continue beyond the vaccination time period and could be an effect of continued pembrolizumab treatment beyond the vaccination phase (Figure S4D, green).

Neoantigen-specific CD4 $^{+}$ T cell responses generated post-vaccination have an activated effector phenotype

To further elucidate the role of vaccine-induced CD4 $^{+}$ T cells induced in the patients, we generated a detailed transcriptomic and clonotype atlas of these cells by using a combination of single-cell sequencing techniques, including TCR- sequencing and cellular indexing of transcriptomes and epitopes by sequencing (CITE-seq). Using these methodologies, we were able to overlay detailed single-cell-level TCR-seq data with protein and gene expression analysis comparing neoantigen-specific CD4 $^{+}$ T cells (tetramer $^{+}$) with bulk (tetramer $^{-}$) CD4 $^{+}$ T cells for five patients from peripheral blood at the post-vaccination time point (Figures 6A and S5A). The addition of protein expression analysis using CITE-seq to standard gene expression strengthened the clustering analysis (Figures S5B and S5C). Three of these patients achieved PFS-9 on the study and two did not. We chose CD4 $^{+}$ T cell responses representative of all of the responses in a patient based on availability of class II tetramers and the magnitude of the response yielding enough cells for detailed analysis. To perform these analyses, neoantigen-specific CD4 $^{+}$ T cells were sorted using MHC class II multimers as shown in Figure 6A (right). Unsupervised clustering of all CD4 $^{+}$ T cells across the five patients revealed commonly observed T cell subsets determined based on the expression profiles, such as naive CD4 $^{+}$ T cells, central memory, T regulatory cells (Treg), and effector CD4 $^{+}$ T cells (Figure 6B). Additional analysis demonstrated that the tetramer $^{+}$ cells for each of the 5 patients analyzed cluster separately from the tetramer $^{-}$ CD4 $^{+}$ T cell population, indicating a difference in transcriptomic and protein profiles (Figure 6C). Indeed, tetramer $^{+}$ CD4 $^{+}$ T cells fall into the “effector activation/exhaustion” (eff act/exh), “effector proliferation” (eff prolif), and “cytotoxic” clusters at a greater frequency than the tetramer $^{-}$ CD4 $^{+}$ T cells, while tetramer $^{-}$ cells fall into clusters of “naive,” “central memory,” and “effector memory” (eff memory) cells (Figure 6D). Differential gene expression analysis further underscored the difference in cluster distribution and phenotypes between tetramer $^{+}$ and tetramer $^{-}$ populations. We found that ZEB2, PDCD1, TOX, TIGT, CXCR3, ITGB1, GZMA, and ICOS were all within the top 100 genes significantly upregulated in the tetramer $^{+}$ (neoantigen-specific) CD4 $^{+}$ T cell populations (Tables S4 and S5). In addition, when the clonality of the TCR repertoire was compared across the tetramer $^{+}$ and tetramer $^{-}$ populations as measured by the Gini coefficient (Kirsch

Figure 3. Correlates with clinical response are observed pre-treatment in the tumor microenvironment (TME), including T cell infiltration, MHC class II expression, and TCR diversity

- (A) Correlation of CD4 $^{+}$ (top) and CD8 $^{+}$ (bottom) T cells per square millimeter either outside the tumor (left) or inside the tumor (right) in patient tumor biopsy material by multiplex immunofluorescence at the pre-treatment time point with PFS in months. Pearson’s correlation coefficient (R) and the associated p value are indicated.
- (B) Representative images of immunofluorescence analysis of CD4 $^{+}$ and CD8 $^{+}$ T cells in patient tumor biopsy material are shown for 1 patient with no PFS-9 (2L3) and 1 patient with PFS-9 (2L5) stained with DAPI (blue), CD3 (red), CD4 (green), CD8 (white), and PanCK (cyan). White arrows indicate CD8 $^{+}$ T cells around the tumor area, and yellow arrows indicate CD4 $^{+}$ T cells infiltrating into the TME.
- (C) Correlation of HLA class II gene expression in the tumor biopsy at the pre-treatment time point, with PFS in months. Pearson’s correlation coefficient (R) and the associated p value are indicated.
- (D) Representative images of MHC class II expression by multiplex immunofluorescence in patient tumor biopsy material are shown for 1 patient with no PFS-9 (2L3) and 1 patient with PFS-9 (2L5) stained with HLA-DR/DP/DQ (red), PanCK (green), DAPI (blue), CD11c (white), and CD14 (yellow). Individual channel images for patient 2L5 are shown below multiplex images for HLA-DR/DP/DQ, CD14, CD11c, and PanCK. White arrows denote HLA-DR/DP/DQ $^{+}$ CD11c $^{+}$ CD14 $^{+}$ cells, and yellow arrow denote HLA-DR/DP/DQ $^{+}$ CD11c $^{-}$ CD14 $^{+}$ cells.
- (E) Analysis of Shannon’s entropy (left) and unique amino acid (UniAA) count (right) in the tumor biopsy at the pre-treatment time point and correlation with PFS in months. Pearson’s correlation coefficient (R) and the associated p value are indicated.
- (F) Analyses of Shannon’s entropy (left) and UniAA count (right) at the pre-treatment (week 0), pre-vaccine (week 12), and post-vaccine (week 24) time points in tumor biopsy material are shown, with PFS-9 patients represented in green, and no-PFS-9 patients represented in blue.

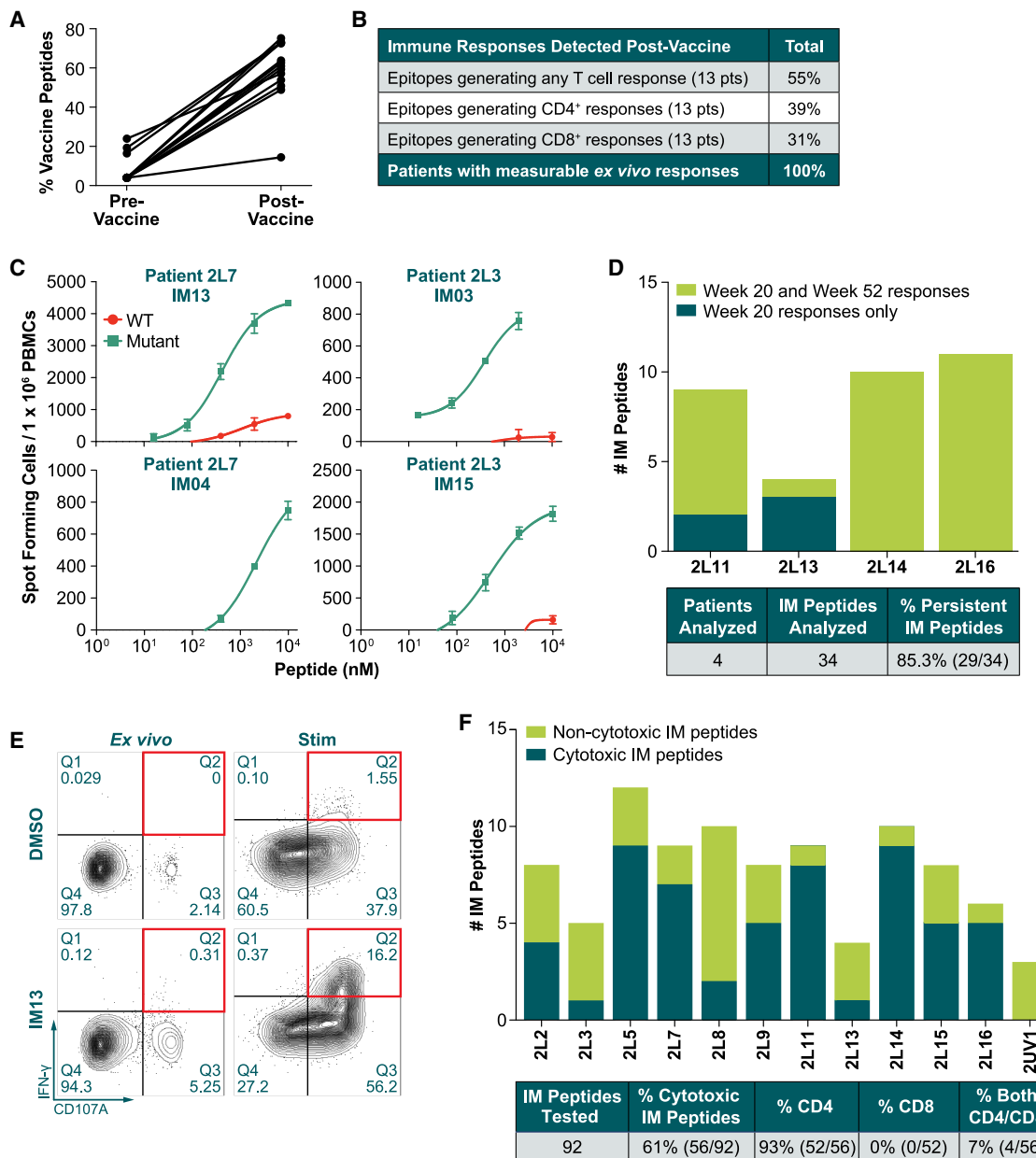


Figure 4. NEO-PV-01 plus chemotherapy and anti-PD-1 induces neoantigen-reactive T cell responses that are neo-epitope specific, persistent, and show cytotoxic potential

(A) Percentage of all NEO-PV-01 vaccinating peptides that elicited IFN- γ responses in serial peripheral blood mononuclear cells (PBMCs) at the indicated time points.

(B) Table summarizing overall immune responses detected for the 13 patients (pts) analyzed, also characterized as percent CD4⁺ or CD8⁺ responses.

(C and D) Specificity of immune responses as measured by IFN- γ ELISpot assay to mutant peptides (green) versus wild-type peptides (red) across a range of peptide concentrations. Representative responses from patient 2L7 (IM13 and IM04) and 2L3 (IM03 and IM15) are shown. Aggregate data are represented as means \pm SEMs. (D) Persistence of immune responses induced by IM peptides, as measured by IFN- γ ELISpot assay in PBMCs collected at week 52 after the initiation of chemotherapy plus anti-PD-1 therapy. The data are represented as stacked columns for individual patients, with responses detected at both weeks 20 and 52 shown in light green, and responses detected only at week 20 shown in dark green.

(E and F) Cytotoxic potential of NEO-PV-01-generated immune response as measured by the surface expression of the marker CD107a in combination with intracellular IFN- γ expression at the post-vaccine time point. (E) Representative flow plots for patient 2L7 are shown, comparing peptide recall (bottom) with DMSO recall (top) in both the *ex vivo* (left) and 5-day stimulation (right) assay design. The data are summarized in (F) and represented as stacked columns for individual patients, with positive (cytotoxic potential) responses shown in dark green, and negative (no cytotoxic potential) responses shown in light green. The table below summarizes the responses detected for all of the patients analyzed, and categorizes responses as either CD4⁺, CD8⁺ or both. See also Figures S2 and S3 and Table S3.

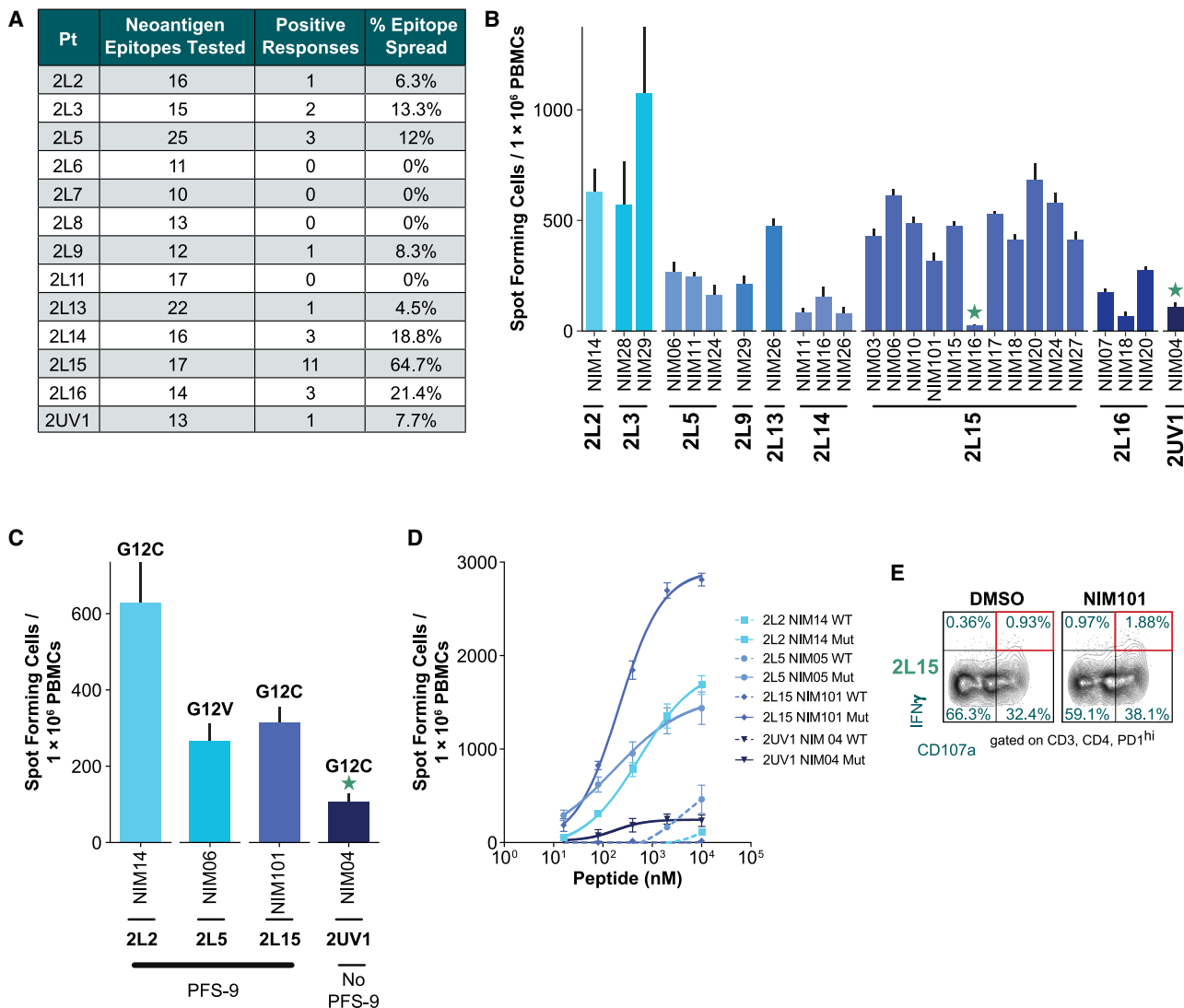


Figure 5. NEO-PV-01 plus chemotherapy and anti-PD-1 induces epitope spread responses in most patients analyzed, with mutant KRAS responses observed in multiple patients

(A) Epitope spread was measured in 13 patients. Reactivity of the post-vaccine PBMCs against a range of 10–25 predicted neoantigen peptides that were not included in the vaccine were tested by IFN- γ ELISpot assay. Responses characterized as epitope spread were detected only at the post-vaccine time point (week 20) and were not detected at the pre-vaccine time point (week 10).

(B) T cell responses to individual non-immunizing (NIM) peptides across 9 patients at the post-vaccination time point are shown. NIM peptides that did not elicit reactivity post-vaccination are not shown. Each NIM peptide was tested for the generation of an immune response using overlapping assay peptides, and the assay peptide that generated the maximum response in either the ex vivo assay or 5-day assay is shown. Responses with green stars denote ex vivo responses.

(C) Four patients elicited mutKRAS-specific epitope spread responses as determined by IFN- γ ELISpot assay. PFS-9 status of each patient is denoted below the graph, and specific G12 mutation denoted above the graph. Responses with green stars denote ex vivo responses.

(D) Specificity of immune responses as measured by IFN- γ ELISpot assay to mutant peptides (solid lines) versus wild-type peptides (dotted lines) across a range of peptide concentrations for each of the 4 patients where an epitope spread response to mutKRAS was observed.

(E) Surface expression of the cytolytic marker CD107a (x axis) and intracellular expression of IFN- γ (y axis) is shown by fluorescence-activated cell sorting (FACS) analysis for the mutKRAS-specific epitope spread response observed for patient 2L15. Individual plots depict control (DMSO) on the left and NIM peptide on the right. Positivity in this assay was determined as a >1.5-fold stimulation over DMSO control in the double-positive gate. Parent gates are indicated below the pair of FACS plots. Aggregate data in (B)–(D) are represented as means \pm SEMs.

See also Figure S4 and Table S1.

et al. 2015; Poran et al., 2020), we observed increased clonality of the neoantigen-specific tetramer $^{+}$ populations for each of the 5 patients when compared to the tetramer $^{-}$ CD4 $^{+}$ T cell population (Figure 6E).

To better understand the difference in phenotype of effector cells specifically within the vaccine-generated neoantigen-specific CD4 $^{+}$ T effector cell (tetramer $^{+}$) and other effector cell (tetramer $^{-}$) populations, all of the effector cells were identified as

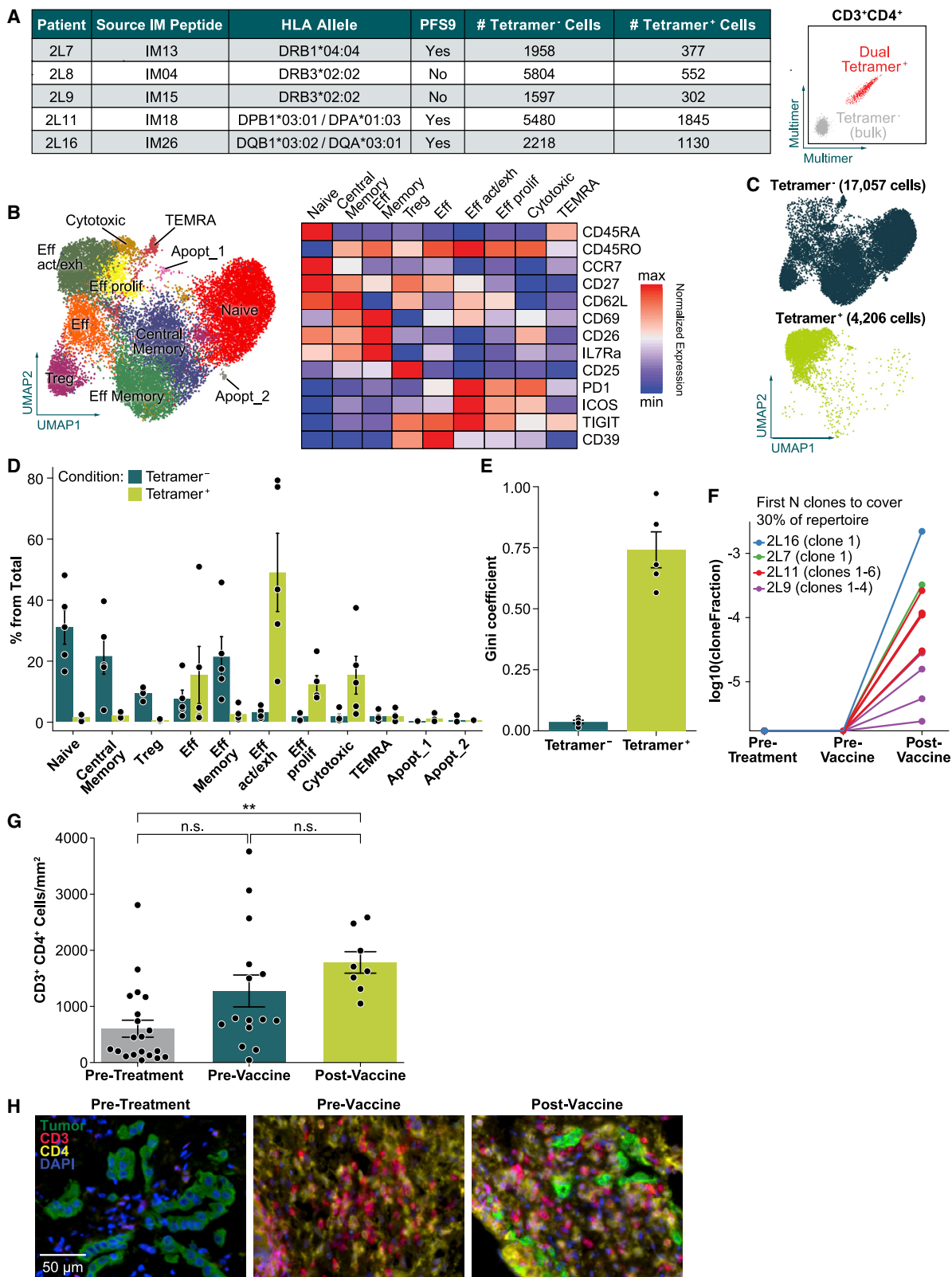


Figure 6. Neoantigen-specific CD4⁺ T cell responses share an activated effector phenotype in the periphery following vaccination

(A) Table summarizing the 5 patients analyzed using a combination of multimer-based sorting of neoantigen-specific CD4⁺ T cells (representative flow panel at right), CITE-seq, TCR-seq, and gene expression analysis.

(legend continued on next page)

being CD45RO⁺CD45RA⁻CD62L^{lo}CCR7^{lo}, and subject to unsupervised clustering (Figures S5D and S5E). This analysis revealed 5 unique clusters, with the tetramer⁻ cells falling mainly in clusters 1 and 2, and tetramer⁺ cells falling mainly in clusters 0, 3, and 4 (Figures S5E and S5F). Expression profiles of each cluster revealed that tetramer⁻ effector cells demonstrate an effector memory phenotype (*TCF7*, *IL7R*, *CCR7*), whereas the tetramer⁺/vaccine-specific CD4⁺ T effector cells demonstrate activation/exhaustion (*PDCD1*, *ICOS*, *TIGIT*, *TOX*) or cytotoxic (*PFR1*, *GNLY*) phenotypes (Figure S5G).

Additional analysis of CD4⁺ neoantigen-specific T cell responses was performed using a combination of MHC class II multimer staining and phenotypic analysis by flow cytometry for 10 patients (Figure S6). Overall, the flow analysis was consistent with the CITE-seq analysis described in Figures 6A–6C, in which the majority of neoantigen-specific CD4⁺ T cells demonstrate an effector phenotype when compared to tetramer⁻ CD4⁺ T cells.

Clustering analysis of only the tetramer⁺ CD4⁺ T cells was performed to determine whether there are phenotypic differences in the neoantigen-specific CD4⁺ T cell clones both within an individual patient and between patients (Figure S7A). Markers representative of each identified cluster and T cell phenotype are shown in the corresponding uniform manifold approximation and projection (UMAP) (Figure S7B). Gene and protein expression profiles used for clustering analysis are shown in Figures S7C and S7D, respectively. The abundance of each phenotype observed on a per-patient level is shown in Figure S7E. Furthermore, we assessed the phenotypes of T cells belonging to the most abundant TCR clones coming from the top 30% of each patient's tetramer⁺ TCR repertoire. We observed consistency in phenotypes across clones within a patient, but varying phenotypes when comparing across patients. (Figure S7F). To confirm specificity of the CD4⁺ TCR clones to the predicted peptide:MHC class II allele combination, four of the top TCRs identified from each single-cell TCR sequencing result across four patients were validated by cloning the individual TCR into the CD4⁺ Jurkat cell line, followed by co-culture with patient-matched antigen-presenting cells (APCs) loaded with either the mutated neoantigen peptide corresponding to the vaccine or the relevant wild-type peptide. Cloned TCRs for patients 2L7, 2L8, and 2L16 (recognizing the vaccine peptides IM13, IM04, and IM26, respectively) resulted in secretion of interleukin-2 (IL-2) only in response to the mutated neoantigen peptide, and not the corresponding wild-type peptide (Fig-

ure S7G). No wild-type peptide was available as a control for patient 2L11, in which the vaccine peptide (IM18) targets a frameshift mutation (Figure S7G).

To validate that the neoantigen-specific tetramer⁺ CD4⁺ T cells being observed were present in the patient's peripheral blood only after vaccination, we performed bulk TCR sequencing of CD3⁺-enriched patient PBMCs at the pre-treatment, pre-vaccine, and post-vaccine time points and quantified the abundance of the TCR clones covering the top 30% of the repertoire in concordance with the single-cell TCR sequencing discussed previously (Figure S7A). We detected each of these dominant clones only at the post-vaccination time point (Figure 6F). We were not able to assess any of the top 4 clones for patient 2L8 in the bulk TCR sequencing due to the lack of available patient material. In addition, immunohistochemical analysis of longitudinal tumor biopsies obtained at pre-treatment, pre-vaccine, and post-vaccine time points was performed where available, revealing a significant increase in the presence of CD4⁺ T cells at the post-vaccine time point when compared to the pre-treatment time point (Figures 6G and 6H). This increase was observed only in CD4⁺ T cells and not in CD8⁺ T cells (Figure S7H). The increase in CD4⁺ T cells was also seen at the pre-vaccine time point and continued to increase at the post-vaccine time point. Representative images from the three time points from patient 2L7 show a marked increase in CD4⁺ T cell infiltration into the tumor following the initiation of treatment in both the pre-vaccine and post-vaccine time points (Figure 6H). To address whether vaccine-induced T cells can be found in the post-treatment biopsy, we looked for the TCR clones that were exclusively found in the post-vaccine biopsy of patient 2L7 and 2L9 and compared the presence of these clones in the periphery across the three time points of pre-treatment, pre-vaccination, and post-vaccination. This identified two distinct sets of clones, ones that expanded upon vaccination in the periphery (Figure S7I, red) and ones that were detected exclusively at the post-vaccination time point in the periphery (Figure S7I, blue), suggesting that vaccine-induced T cells in the periphery can traffic to the post-vaccination tumor. Although the specificities of these tumor-penetrating clones are currently unknown, we presume a majority of these clones to be induced by the vaccine due to their expansion/detection only upon vaccination.

DISCUSSION

In this report of a Phase I study in non-squamous NSCLC, we have further tested the utility of targeting neoantigens in the

- (B) Unsupervised clustering (left) and heatmap (right) of normalized expression used for clustering analysis of tetramer⁺ and tetramer⁻ CD4⁺ T cell samples from the 5 patients.
- (C) Unsupervised clustering plots separated to visualize tetramer⁻ cells (top) and tetramer⁺ cells (bottom) from the 5 patients.
- (D) Proportions of each UMAP cluster comparing tetramer⁺ and tetramer⁻ populations.
- (E) Measurement of the Gini coefficient (as an indicator of TCR repertoire clonality) for both tetramer⁺ and tetramer⁻ populations. Each dot represents an individual patient.
- (F) Measurement of clonotypes covering the top 30% of the TCR repertoire of tetramer⁺ CD4⁺ T cells that were detected by single-cell TCR sequencing using bulk TCR-seq data across the pre-treatment, pre-vaccine, and post-vaccine timepoints.
- (G) Measurement of the number of CD3⁺CD4⁺ T cells per square millimeter of tumor biopsy tissue using multiplex immunofluorescence at the pre-treatment, pre-vaccine, and post-vaccine time points when available.
- (H) Representative immunofluorescence images for patient 2L7 (PFS-9) at the pre-treatment (left), pre-vaccine (center), and post-vaccine (right) time points are shown, stained with DAPI (blue), CD3 (red), CD4 (yellow), and PanCK (green). Longitudinal biopsies were from the same lung lesion for this patient. Aggregate data in (D), (E), and (G) are represented as means \pm SEMs.

See also Figures S5–S7 and Tables S4 and S5.

context of immune checkpoint and chemotherapy combination as first-line treatment. Despite the recent advances in the treatment of metastatic NSCLC using immunochemotherapy (Gandhi et al., 2018; Gadgeel et al., 2020; Rodríguez-Abreu et al., 2021), the median OS of metastatic NSCLC remains less than 3 years (Wang et al., 2021), warranting the need to improve upon the current standard of care. Our report of personalized neoantigen vaccine in this setting evaluates the safety, immunogenicity, and potential clinical benefit in this patient group.

The clinical data from this study indicate that a personalized neoantigen-based vaccination strategy is feasible and safe as a first-line treatment in NSCLC in combination with standard of care chemotherapy plus pembrolizumab. The single-arm design of the trial does not allow attribution of clinical responses specifically to the vaccine since it was administered in combination with anti-PD-1 and chemotherapy. A study that could serve as a historical comparator is KEYNOTE 189 (Gandhi et al., 2018; Gadgeel et al., 2020). However, this study could not be directly compared to our study, given the differences in the patient populations and the treatment regimens. Patients in the KEYNOTE 189 study received maintenance chemotherapy, while patients in the NT002 study received NEO-PV-01 alone after the initial four cycles of chemotherapy and checkpoint inhibitor. In addition, the NT002 vaccinated study cohort had a higher ratio of female to male patients and lower relative tumor PD-L1 expression, each of which can be associated with inferior clinical outcomes to the combination of immunotherapy with chemotherapy (Conforti et al., 2018; Gandhi et al., 2018).

Approximately 45% of the enrolled patients were unable to proceed to vaccination due to progressive disease, the inability to manufacture vaccine due to low tumor content in the biopsy, or insufficient mutations leading to a low number of high-quality neoantigens. Steps to mitigate such failures would include improved vaccine production timelines, evaluation of tumor mutational burden (TMB) using some of the emerging technologies from cell-free DNA, and using a vaccine format such as mRNA that may be faster to manufacture and administer as well as overcome the solubility limitation of synthetic long peptides.

With respect to the immunogenicity of the personalized vaccine in the context of immunochemotherapy, we did not observe it to be different from our previously reported immunogenicity of NEO-PV-01 in combination with anti-PD-1 alone (Ott et al., 2020). It is encouraging to see that despite receiving an immunosuppressive chemotherapy regimen before vaccination, a robust immune response was generated to the vaccine in all of the patients analyzed, with both CD4⁺ and CD8⁺ responses being generated. Interestingly, a large majority of the vaccine-induced cytotoxic responses were CD4⁺ T cells. This is in contrast to our previous study, in which we observed both CD4⁺ and CD8⁺ cytotoxic T cells generated in response to NEO-PV-01 vaccination (Ott et al., 2020) in combination with nivolumab alone. The differences observed with the previous study could be attributed to the differences in treatment combination or may be because this was a cohort of exclusively first-line NSCLC cancer patients. In addition, we observe robust MHC II expression in the TME of this patient cohort, particularly at the post-vaccination time point. This suggests the presence of a microenvironment in favor

of developing CD4⁺ T cell responses. Skewing toward CD4⁺ T cell responses has been reported previously in the setting of neoantigen vaccine as well (Ott et al., 2017; Sahin et al., 2017).

The role of tumor-specific cytolytic CD4⁺ T cells has only begun to emerge, with some of the early data focused on identification of these cells in the context of pre-treatment biopsies and its predictive value for response to checkpoint therapy (Kitano et al., 2013; Kagamu et al., 2020; Oh et al., 2020). The use of single-cell sequencing technologies and multiparametric flow-based analysis has further enabled the detailed characterization and definition of gene expression patterns associated with such cytotoxic CD4⁺ T cells (Patil et al., 2018; Ma et al., 2021; Nicolet et al. 2021). Our data demonstrate the generation of such effector and cytolytic CD4⁺ T cells upon vaccination with a personalized vaccine. Of note, the CD4⁺ neoantigen T cells generated in the study were not of the Treg phenotype (they did not express Foxp3) and instead had a distinct effector cytotoxic phenotype that could mediate tumor cell killing. In addition, the increase in CD4⁺ T cells and not CD8⁺ T cells post-initiation of treatment emphasizes a critical role for CD4⁺ T cell compartment in tumor control.

Another aspect of our study is the generation of epitope spread responses in multiple patients. Of particular interest are the epitope spread responses seen toward common driver mutations KRAS G12C and KRAS G12V across multiple patients. Preexisting immune responses to KRAS G12V and KRAS G12D mutation have been reported in a cohort of patients from colorectal cancer and a NSCLC patient previously (Cafri et al., 2019; Veatch et al., 2019). Identification of such immune responses in our study provides additional data on KRAS mutation-specific T cells that can be further developed for T cell or vaccine-based therapies.

A limitation of our study is its single-arm design. Since the vaccine was administered in combination with anti-PD-1 and chemotherapy, the clinical responses, epitope spread, and immunogenicity cannot be solely attributed to the vaccine alone. Randomized trials of neoantigen therapy in combination with anti-PD-1 and chemotherapy versus immunochemotherapy alone will be necessary to confirm these findings and determine the specific contribution of the personalized vaccine.

In summary, we demonstrate the safety, feasibility, and generation of desired immune responses upon treatment with personalized neoantigen-based vaccine in combination with anti-PD-1 and chemotherapy as a first-line treatment in NSCLC. Identification of potential tumor biomarkers holds promise for selecting patients in further randomized trials. These trials will be required to further refine the use of personalized neoantigen vaccine in combination with immunochemotherapy as a first-line treatment in NSCLC.

STAR★METHODS

Detailed methods are provided in the online version of this paper and include the following:

- [KEY RESOURCES TABLE](#)
- [RESOURCE AVAILABILITY](#)
 - Lead contact
 - Materials availability

- Data and code availability
- **EXPERIMENTAL MODEL AND SUBJECT DETAILS**
 - NT-002 study design
 - Treatment regimen
 - Eligibility
 - Clinical assessments
 - Patient samples
- **METHOD DETAILS**
 - Generation of NEO-PV-01
 - Peptide synthesis for immunological assays
 - Personalized ctDNA assays
 - Detection of neoantigen-specific immune responses
 - IFN γ ELISpot assay
 - Characterization of CD4 $^{+}$ /CD8 $^{+}$ T cell responses
 - CD107a mobilization assay
 - MHCII protein expression, purification, and peptide exchange
 - Multimer generation and staining
 - Phenotyping of multimer $^{+}$ CD4 $^{+}$ T cells
 - RNA extraction from FFPE tumors and PBMCs
 - Gene expression analysis
 - TCR library preparation and sequencing
 - TCR repertoire generation
 - TCR repertoire diversity/clonality analysis
 - Single-cell RNA sequencing of neoantigen-specific CD4 $^{+}$ T cells using HLA class II multimer staining
 - Single-cell RNA sequencing data analysis
 - Cloning of neoantigen-specific TCRs
 - MultiOmyx staining
 - Multiplex IHC staining protocol
 - Multispectral analysis
 - Statistical analysis
- **ADDITIONAL RESOURCES**

SUPPLEMENTAL INFORMATION

Supplemental information can be found online at <https://doi.org/10.1016/j.ccel.2022.08.003>.

ACKNOWLEDGMENTS

We thank all of the patients and their families who participated in the study. We are grateful to all of the members of BioNTech US for their support and assistance on the study. We thank April Lamb and Jennifer Tepper for clinical operations; Marc Wolfgang, Scott White, Stephen Crimlisk, and Yeimi Garcia for technical operations; Jonathan McGee, Heidi Jackson, Madeline Worob, Yuting Huang, Daniel Kallin, and Alyssa Kruithof for peptide synthesis and manufacturing process development; Janani Sridar and Paul Turcott for tetramer reagent generation; Riley Curran, Samantha Turnbull, Rana Besada, Ben Trapp, Julian Scherer, and Gauri Mahimkar for immune analysis study support; Miles Kirsch and Dewi Harjanto for bioinformatics support; Kerry Chios and Nidal El-Assi for lab operation support and biobank management; Zhengping Huang and Amy Wanamaker for informatics support and clinical data management; Mominul Islam for biostatistics support; Andrew Finlayson for careful review; and Hugh O'Dowd for support and guidance on the study. We thank Merck for the pembrolizumab supply. The study was sponsored by Neon Therapeutics/BioNTech US.

AUTHOR CONTRIBUTIONS

M.M.A., L.S., and R.B.G., conceptualization and implementation of the study; M.M.A., R.G., D.R.S., and E.B.G., clinical investigators on the study; K.N.B., M.E.B., A.P., J.H.S., V.K., E.E., S.R., T.E.S., and M.S.R., biomarker and

sequencing analysis; K.N.B., V.K., and S.R., patient immune analysis, J.Z.D., peptide synthesis and purification; J.S. and R.V., tetramer reagent generation; M.A.M. and K.M., clinical operations and program management; Z.S.K., bios-statistics support; M.mD.M., medical monitor on the study; M.M.A., K.N.B., M.D.M., L.S., and R.B.G., manuscript preparation, with inputs from all of the authors.

DECLARATION OF INTERESTS

M.M.A., research grants (to institution): Genentech, Lilly, Bristol-Myers Squibb, AstraZeneca; consulting/advisory board fees, Genentech, Bristol-Myers Squibb, Merck, AstraZeneca, AbbVie, Neon, Achilles, Maverick, Blueprint Medicine, Hengrui, Syndax, Ariad, Nektar, Gritstone, ArcherDX, Mirati, NextCure, Novartis, EMD Serono, Panvaxal/NovaRx, Foundation Medicine. R.G., advisory role, Precisa Lung, Merck, Jacobio. D.R.S., research grants (to institution), Aeglea, Agios, Apollomics, Arcus, Arrys, Astellas, AstraZeneca, Bayer, BeiGene, Therapeutics, BioNTech RNA Pharmaceuticals, Blueprint Medicine, Boehringer-Ingelheim, Bristol-Myers Squibb, Calithera, Celldex, Clovis, Cyteir, Daiichi Sankyo, Biopharma, Eisai, Elevation Oncology, EMD Serono, Evelo Biosciences, G1, Roche/Genentech, GlaxoSmithKline, GRAIL, Hutchison MediPharma, ImClone Systems, Incyte, ImmunoGen, Ipsen, Janssen, Kronos Bio, Loxo Oncology, MacroGenics, MedImmune, Merck, Molecular Partners, Molecular Template, Nektar, Novartis, Novocure, Oncologie, Pfizer, PTC, PureTech Health, Razor Genomics, Repare, Rgenix, Takeda, Tesaro, Tizona Therapeutics, Transgene, University of Texas Southwestern, Verastem; consulting/advisory board (to institution), Amgen, AstraZeneca, Bristol-Myers Squibb, Curio Science, EMD Serono, Evidera, Exelixis, GlaxoSmithKline, IntelliSphere, Ipsen, Janssen, Jazz, Lilly, Mirati, Molecular Templates, Novartis, Novocure, Pfizer, Puma Biotechnology, Regeneron, Roche/Genentech, Sanofi-Aventis. EBG: Consulting or Advisory Role: ABL Bio, Boehringer Ingelheim, Bristol-Myers Squibb, Dracen, Eisai, Eli Lilly, EMD Serono, Gilead, GSK, Merck, Natera, Novartis, Personalis, Regeneron, Sanofi, Shionogi, Xilio; grant/research support, ABL Bio, AstraZeneca, Bristol-Myers Squibb, Dynavax Technologies, EMD Serono, Genentech, Iovance Biotherapeutics, Eli Lilly, Merck, Mirati, Neon, Novartis. R.B.G., Board of Directors, Alkermes plc, Infinity Pharmaceuticals, and Zai Laboratory, and Scientific Advisory Board, Leap Therapeutics; consultant Third Rock Ventures, stockholder and employee of BioNTech US. H.S., employee of Natera, with stock/options to own stock in the company. K.N.B., M.E.B., A.P., J.H.S., V.K., E.E., J.S., S.R., R.V., T.E.S., J.Z.D., M.A.M., K.M., M.S.R., Z.S.K., M.D.M., and L.S., stockholder and either current or past employees of Neon Therapeutics/BioNTech US.

Received: February 14, 2022

Revised: June 6, 2022

Accepted: August 2, 2022

Published: August 25, 2022

REFERENCES

- Abbosh, C., Birkbak, N.J., Wilson, G.A., Jamal-Hanjani, M., Constantin, T., Salari, R., Le Quesne, J., Moore, D.A., Veeriah, S., Rosenthal, R., et al. (2017). Phylogenetic ctDNA analysis depicts early-stage lung cancer evolution. *Nature* 545, 446–451. <https://doi.org/10.1038/nature22364>. <https://www.ncbi.nlm.nih.gov/pubmed/28445469>.
- Abelin, J.G., Keskin, D.B., Sarkizova, S., Hartigan, C.R., Zhang, W., Sidney, J., Stevens, J., Lane, W., Zhang, G.L., Eisenhaure, T.M., et al. (2017). Mass spectrometry profiling of HLA-associated peptidomes in mono-allelic cells enables more accurate epitope prediction. *Immunity* 46, 315–326. <https://doi.org/10.1016/j.jimmuni.2017.02.007>.
- Awad, M.M., Gadgeel, S.M., Borghaei, H., Patnaik, A., Yang, J.C.H., Powell, S.F., Gentzler, R.D., Martins, R.G., Stevenson, J.P., Altan, M., et al. (2021). Long-term overall survival from KEYNOTE-021 cohort G: pembrolizumab and carboplatin with or without pembrolizumab as first-line therapy for advanced non-squamous NSCLC. *J. Thorac. Oncol.* 16, 162–168. <https://doi.org/10.1016/j.jtho.2020.09.015>. <https://www.ncbi.nlm.nih.gov/pubmed/33069888>.
- Betts, M.R., Brenchley, J.M., Price, D.A., De Rosa, S.C., Douek, D.C., Roederer, M., and Koup, R.A. (2003). Sensitive and viable identification of

- antigen-specific CD8+ T cells by a flow cytometric assay for degranulation. *J. Immunol. Methods* 281, 65–78. [https://doi.org/10.1016/s0022-1759\(03\)00265-5](https://doi.org/10.1016/s0022-1759(03)00265-5). <https://www.ncbi.nlm.nih.gov/pubmed/14580882>.
- Bolotin, D.A., Poslavsky, S., Mitrophanov, I., Shugay, M., Mamedov, I.Z., Putintseva, E.V., and Chudakov, D.M. (2015). MiXCR: software for comprehensive adaptive immunity profiling. *Nat. Methods* 12, 380–381.
- Borghaei, H., Langer, C.J., Paz-Ares, L., Rodríguez-Abreu, D., Halmos, B., Garassino, M.C., Houghton, B., Kurata, T., Cheng, Y., Lin, J., et al. (2020). Pembrolizumab plus chemotherapy versus chemotherapy alone in patients with advanced non-small cell lung cancer without tumor PD-L1 expression: a pooled analysis of 3 randomized controlled trials. *Cancer* 126, 4867–4877. <https://doi.org/10.1002/cncr.33142>. <https://www.ncbi.nlm.nih.gov/pubmed/32914866>.
- Bratman, S.V., Yang, S.Y.C., Lafolla, M.A.J., Liu, Z., Hansen, P.L.B., Lheureux, S., Anna, S., Abdul Razak, A., Shchegrova, S., Louie, M., et al. (2020). Personalized circulating tumor DNA analysis as a predictive biomarker in solid tumor patients treated with pembrolizumab. *Nat. Cancer* 1, 873–881. <https://doi.org/10.1038/s43018-020-0096-5>.
- Cabrita, R., Lauss, M., Sanna, A., Donia, M., Skaarup Larsen, M., Mitra, S., Johansson, I., Phung, B., Harbst, K., Vallon-Christersson, J., et al. (2020). Tertiary lymphoid structures improve immunotherapy and survival in melanoma. *Nature* 577, 561–565. <https://doi.org/10.1038/s41586-019-1914-8>. <https://www.ncbi.nlm.nih.gov/pubmed/31942071>.
- Cafri, G., Yossef, R., Pasetto, A., Deniger, D.C., Lu, Y.C., Parkhurst, M., Gartner, J.J., Jia, L., Ray, S., Ngo, L.T., et al. (2019). Memory T cells targeting oncogenic mutations detected in peripheral blood of epithelial cancer patients. *Nat. Commun.* 10, 449. <https://doi.org/10.1038/s41467-019-08304-z>. <https://www.ncbi.nlm.nih.gov/pubmed/30683863>.
- Carter, S.L., Cibulskis, K., Helman, E., McKenna, A., Shen, H., Zack, T., Laird, P.W., Onofrio, R.C., Winckler, W., Weir, B.A., et al. (2012). Absolute quantification of somatic DNA alterations in human cancer. *Nat. Biotechnol.* 30, 413–421. <https://doi.org/10.1038/nbt.2203>. <https://www.ncbi.nlm.nih.gov/pubmed/22544022>.
- Challis, D., Yu, J., Evani, U.S., Jackson, A.R., Paithankar, S., Coarfa, C., Milosavljevic, A., Gibbs, R.A., and Yu, F. (2012). An integrative variant analysis suite for whole exome next-generation sequencing data. *BMC Bioinf.* 13, 8. <https://doi.org/10.1186/1471-2105-13-8>. <https://www.ncbi.nlm.nih.gov/pubmed/22239737>.
- Christensen, E., Birkenkamp-Demtroder, K., Sethi, H., Shchegrova, S., Salari, R., Nordentoft, I., Wu, H.T., Knudsen, M., Lamy, P., Lindskrog, S.V., et al. (2019). Early detection of metastatic relapse and monitoring of therapeutic efficacy by ultra-deep sequencing of plasma cell-free DNA in patients with urothelial bladder carcinoma. *J. Clin. Oncol.* 37, 1547–1557. <https://doi.org/10.1200/JCO.18.02052>. <https://www.ncbi.nlm.nih.gov/pubmed/31059311>.
- Christoforides, A., Carpten, J.D., Weiss, G.J., Demeure, M.J., Von Hoff, D.D., and Craig, D.W. (2013). Identification of somatic mutations in cancer through Bayesian-based analysis of sequenced genome pairs. *BMC Genom.* 14, 302. <https://doi.org/10.1186/1471-2164-14-302>. <https://www.ncbi.nlm.nih.gov/pubmed/23642077>.
- Cibulskis, K., McKenna, A., Fennell, T., Banks, E., DePristo, M., and Getz, G. (2011). ContEst: estimating cross-contamination of human samples in next-generation sequencing data. *Bioinformatics* 27, 2601–2602. <https://doi.org/10.1093/bioinformatics/btr446>. <https://www.ncbi.nlm.nih.gov/pubmed/21803805>.
- Cohen, C.J., Zhao, Y., Zheng, Z., Rosenberg, S.A., and Morgan, R.A. (2006). Enhanced antitumor activity of murine-human hybrid T-cell receptor (TCR) in human lymphocytes is associated with improved pairing and TCR/CD3 stability. *Cancer Res.* 66, 8878–8886. <https://doi.org/10.1158/0008-5472.CAN-06-1450>. <https://www.ncbi.nlm.nih.gov/pubmed/16951205>.
- Conforti, F., Pala, L., Bagnardi, V., De Pas, T., Martinetti, M., Viale, G., Gelber, R.D., and Goldhirsch, A. (2018). Cancer immunotherapy efficacy and patients' sex: a systematic review and meta-analysis. *Lancet Oncol.* 19, 737–746. [https://doi.org/10.1016/S1470-2045\(18\)30261-4](https://doi.org/10.1016/S1470-2045(18)30261-4). <https://www.ncbi.nlm.nih.gov/pubmed/29778737>.
- Coombes, R.C., Page, K., Salari, R., Hastings, R.K., Armstrong, A., Ahmed, S., Ali, S., Cleator, S., Kenny, L., Stebbing, J., et al. (2019). Personalized detection of circulating tumor DNA antedates breast cancer metastatic recurrence. *Clin. Cancer Res.* 25, 4255–4263. <https://doi.org/10.1158/1078-0432.CCR-18-3663>. <https://www.ncbi.nlm.nih.gov/pubmed/30992300>.
- Corbiere, V., Chapiro, J., Stroobant, V., Ma, W., Lurquin, C., Lethe, B., van Baren, N., Van den Eynde, B.J., Boon, T., and Coulie, P.G. (2011). Antigen spreading contributes to MAGE vaccination-induced regression of melanoma metastases. *Cancer Res.* 71, 1253–1262. <https://doi.org/10.1158/0008-5472.CAN-10-2693>. <https://www.ncbi.nlm.nih.gov/pubmed/21216894>.
- Corcoran, R.B., and Chabner, B.A. (2018). Application of cell-free DNA analysis to cancer treatment. *N. Engl. J. Med.* 379, 1754–1765. <https://doi.org/10.1056/NEJMra1706174>. <https://www.ncbi.nlm.nih.gov/pubmed/30380390>.
- Gadgeel, S., Rodríguez-Abreu, D., Speranza, G., Esteban, E., Felip, E., Dómíne, M., Hui, R., Hochmair, M.J., Clingen, P., Powell, S.F., et al. (2020). Updated analysis from KEYNOTE-189: pembrolizumab or placebo plus pemetrexed and platinum for previously untreated metastatic nonsquamous non-small-cell lung cancer. *J. Clin. Oncol.* 38, 1505–1517. <https://doi.org/10.1200/JCO.19.03136>. <https://www.ncbi.nlm.nih.gov/pubmed/32150489>.
- Gandhi, L., Rodríguez-Abreu, D., Gadgeel, S., Esteban, E., Felip, E., De Angelis, F., Domine, M., Clingen, P., Hochmair, M.J., Powell, S.F., et al. (2018). Pembrolizumab plus chemotherapy in metastatic non-small-cell lung cancer. *N. Engl. J. Med.* 378, 2078–2092. <https://doi.org/10.1056/NEJMoa1801005>. <https://www.ncbi.nlm.nih.gov/pubmed/29658856>.
- Gerdes, M.J., Sevinsky, C.J., Sood, A., Adak, S., Bello, M.O., Bordwell, A., Can, A., Corwin, A., Dinn, S., Filkins, R.J., et al. (2013). Highly multiplexed single-cell analysis of formalin-fixed, paraffin-embedded cancer tissue. *Proc. Natl. Acad. Sci. USA* 110, 11982–11987. <https://doi.org/10.1073/pnas.1300136110>. <https://www.ncbi.nlm.nih.gov/pubmed/23818604>.
- Gu, Z., Eils, R., and Schlesner, M. (2016). Complex heatmaps reveal patterns and correlations in multidimensional genomic data. *Bioinformatics* 32, 2847–2849. <https://doi.org/10.1093/bioinformatics/btw313>. <https://www.ncbi.nlm.nih.gov/pubmed/27207943>.
- Haas, B.J., Dobin, A., Stransky, N., Li, B., Yang, X., Tickle, T., Bankapur, A., Ganote, C., Doak, T.G., Pochet, N., Sun, J., Wu, C.J., Gingeras, T.R., and Regev, A. (2017). STAR-fusion: fast and accurate fusion transcript detection from RNA-Seq. *Preprint bioRxiv*. <https://doi.org/10.1101/120295>.
- Hanson, A.L., Nel, H.J., Bradbury, L., Phipps, J., Thomas, R., Lê Cao, K., Kenna, T.J., and Brown, M.A. (2020). Altered repertoire diversity and disease-associated clonal expansions revealed by T cell receptor immuno-sequencing in ankylosing spondylitis patients. *Arthritis Rheumatol.* 72, 1289–1302. <https://doi.org/10.1002/art.41252>. <https://www.ncbi.nlm.nih.gov/pubmed/32162785>.
- Hellmann, M.D., Nathanson, T., Rizvi, H., Creelan, B.C., Sanchez-Vega, F., Ahuja, A., Ni, A., Novik, J.B., Mangarin, L.M., Abu-Akeel, M., et al. (2018). Genomic features of response to combination immunotherapy in patients with advanced non-small-cell lung cancer. *Cancer Cell* 33, 843–852.e4. <https://doi.org/10.1016/j.ccr.2018.03.018>.
- Hellmann, M.D., Paz-Ares, L., Bernabe Caro, R., Zurawski, B., Kim, S.W., Carcereny Costa, E., Park, K., Alexandru, A., Lupinacci, L., de la Mora Jimenez, E., et al. (2019). Nivolumab plus ipilimumab in advanced non-small-cell lung cancer. *N. Engl. J. Med.* 381, 2020–2031. <https://doi.org/10.1056/NEJMoa1910231>. <https://www.ncbi.nlm.nih.gov/pubmed/31562796>.
- Helmink, B.A., Reddy, S.M., Gao, J., Zhang, S., Basar, R., Thakur, R., Yizhak, K., Sade-Feldman, M., Blando, J., Han, G., et al. (2020). B cells and tertiary lymphoid structures promote immunotherapy response. *Nature* 577, 549–555. <https://doi.org/10.1038/s41586-019-1922-8>. <https://www.ncbi.nlm.nih.gov/pubmed/31942075>.
- Hilf, N., Kuttruff-Coqui, S., Frenzel, K., Bukur, V., Stevanovic, S., Gouttefangeas, C., Platten, M., Tabatabai, G., Dutoit, V., van der Burg, S.H., et al. (2019). Actively personalized vaccination trial for newly diagnosed glioblastoma. *Nature* 565, 240–245. <https://doi.org/10.1038/s41586-018-0810-y>. <https://www.ncbi.nlm.nih.gov/pubmed/30568303>.
- Hu, Z., Leet, D.E., Allesøe, R.L., Oliveira, G., Li, S., Luoma, A.M., Liu, J., Forman, J., Huang, T., Iorgulescu, J.B., et al. (2021). Personal neoantigen vaccines induce persistent memory T cell responses and epitope spreading in

- patients with melanoma. *Nat. Med.* 27, 515–525. <https://doi.org/10.1038/s41591-020-01206-4>. <https://www.ncbi.nlm.nih.gov/pubmed/33479501>.
- Jia, Q., Zhou, J., Chen, G., Shi, Y., Yu, H., Guan, P., Lin, R., Jiang, N., Yu, P., Li, Q.J., and Wan, Y. (2015). Diversity index of mucosal resident T lymphocyte repertoire predicts clinical prognosis in gastric cancer. *OncolImmunology* 4, e1001230. <https://doi.org/10.1080/2162402X.2014.1001230>. <https://www.ncbi.nlm.nih.gov/pubmed/26137399>.
- Kagamu, H., Kitano, S., Yamaguchi, O., Yoshimura, K., Horimoto, K., Kitazawa, M., Fukui, K., Shiono, A., Mouri, A., Nishihara, F., et al. (2020). CD4+ T-cell immunity in the peripheral blood correlates with response to anti-PD-1 therapy. *Cancer Immunol. Res.* 8, 334–344. <https://doi.org/10.1158/2326-6066.CIR-19-0574>. <https://www.ncbi.nlm.nih.gov/pubmed/31871122>.
- Keskin, D.B., Anandappa, A.J., Sun, J., Tirosh, I., Mathewson, N.D., Li, S., Oliveira, G., Giobbie-Hurder, A., Felt, K., Gjini, E., et al. (2019). Neoantigen vaccine generates intratumoral T cell responses in phase Ib glioblastoma trial. *Nature* 565, 234–239. <https://doi.org/10.1038/s41586-018-0792-9>. <https://www.ncbi.nlm.nih.gov/pubmed/30568305>.
- Kirsch, I., Vignali, M., and Robins, H. (2015). T-cell receptor profiling in cancer. *Mol. Oncol.* 9, 2063–2070. <https://doi.org/10.1016/j.molonc.2015.09.003>. <https://www.ncbi.nlm.nih.gov/pubmed/26404496>.
- Kitano, S., Tsuji, T., Liu, C., Hirschhorn-Cymerman, D., Kyi, C., Mu, Z., Allison, J.P., Gnijatic, S., Yuan, J.D., and Wolchok, J.D. (2013). Enhancement of tumor-reactive cytotoxic CD4+ T cell responses after ipilimumab treatment in four advanced melanoma patients. *Cancer Immunol. Res.* 1, 235–244. <https://doi.org/10.1158/2326-6066.CIR-13-0068>. <https://www.ncbi.nlm.nih.gov/pubmed/24396833>.
- Koboldt, D.C., Zhang, Q., Larson, D.E., Shen, D., McLellan, M.D., Lin, L., Miller, C.A., Mardis, E.R., Ding, L., and Wilson, R.K. (2012). VarScan 2: somatic mutation and copy number alteration discovery in cancer by exome sequencing. *Genome Res.* 22, 568–576. <https://doi.org/10.1101/gr.129684.111>. <https://www.ncbi.nlm.nih.gov/pubmed/22300766>.
- Korsunsky, I., Millard, N., Fan, J., Slowikowski, K., Zhang, F., Wei, K., Baglaenko, Y., Brenner, M., Loh, P.R., and Raychaudhuri, S. (2019). Fast, sensitive and accurate integration of single-cell data with Harmony. *Nat. Methods* 16, 1289–1296. <https://doi.org/10.1038/s41592-019-0619-0>. <https://www.ncbi.nlm.nih.gov/pubmed/31740819>.
- Kreiter, S., Vormehr, M., van de Roemer, N., Diken, M., Lower, M., Diekmann, J., Boegel, S., Schrörer, B., Vascotto, F., Castle, J.C., et al. (2015). Mutant MHC class II epitopes drive therapeutic immune responses to cancer. *Nature* 520, 692–696. <https://doi.org/10.1038/nature14426>. <https://www.ncbi.nlm.nih.gov/pubmed/25901682>.
- Kuball, J., Dossett, M.L., Wolf, M., Ho, W.Y., Voss, R.H., Fowler, C., and Greenberg, P.D. (2007). Facilitating matched pairing and expression of TCR chains introduced into human T cells. *Blood* 109, 2331–2338. <https://doi.org/10.1182/blood-2006-05-023069>. <https://www.ncbi.nlm.nih.gov/pubmed/17082316>.
- Lai, Z., Markovets, A., Ahdesmaki, M., Chapman, B., Hofmann, O., McEwen, R., Johnson, J., Dougherty, B., Barrett, J.C., and Dry, J.R. (2016). VarDict: a novel and versatile variant caller for next-generation sequencing in cancer research. *Nucleic Acids Res.* 44, e108. <https://doi.org/10.1093/nar/gkw227>. <https://www.ncbi.nlm.nih.gov/pubmed/27060149>.
- Li, B., and Dewey, C.N. (2011). RSEM: accurate transcript quantification from RNA-Seq data with or without a reference genome. *BMC Bioinf.* 12, 323. <https://doi.org/10.1186/1471-2105-12-323>. <https://www.ncbi.nlm.nih.gov/pubmed/21816040>.
- Li, H., and Durbin, R. (2009). Fast and accurate short read alignment with Burrows-Wheeler transform. *Bioinformatics* 25, 1754–1760. <https://doi.org/10.1093/bioinformatics/btp324>. <https://www.ncbi.nlm.nih.gov/pubmed/19451168>.
- Luksza, M., Riaz, N., Makarov, V., Balachandran, V.P., Hellmann, M.D., Solovyov, A., Rizvi, N.A., Mergoum, T., Levine, A.J., Chan, T.A., et al. (2017). A neoantigen fitness model predicts tumour response to checkpoint blockade immunotherapy. *Nature* 551, 517–520. <https://doi.org/10.1038/nature24473>. <https://www.ncbi.nlm.nih.gov/pubmed/29132144>.
- Ma, J., Tibbitt, C.A., Georén, S.K., Christian, M., Murrell, B., Cardell, L.O., Bachert, C., and Coquet, J.M. (2021). Single-cell analysis pinpoints distinct populations of cytotoxic CD4 + T cells and an IL-10 + CD109 + T H 2 cell population in nasal polyps. *Sci. Immunol.* 6. <https://doi.org/10.1126/sciimmunol.abg6356>. <https://www.ncbi.nlm.nih.gov/pubmed/34389612>.
- McKenna, A., Hanna, M., Banks, E., Sivachenko, A., Cibulskis, K., Kemberly, A., Garimella, K., Altshuler, D., Gabriel, S., Daly, M., and DePristo, M.A. (2010). The Genome Analysis Toolkit: a MapReduce framework for analyzing next-generation DNA sequencing data. *Genome Res.* 20, 1297–1303. <https://doi.org/10.1101/gr.107524.110>. <https://www.ncbi.nlm.nih.gov/pubmed/20644199>.
- Nicolet, B.P., Guislain, A., and Wolkers, M.C. (2021). CD29 enriches for cytotoxic human CD4+ T cells. *J. Immunol.* 2966–2975. <https://doi.org/10.4049/jimmunol.2100138>. <https://www.ncbi.nlm.nih.gov/pubmed/34782446>.
- Nielsen, M., and Andreatta, M. (2016). NetMHCpan-3.0; improved prediction of binding to MHC class I molecules integrating information from multiple receptor and peptide length datasets. *Genome Med.* 8, 33. <https://doi.org/10.1186/s13073-016-0288-x>. <https://www.ncbi.nlm.nih.gov/pubmed/27029192>.
- Oh, D.Y., Kwek, S.S., Raju, S.S., Li, T., McCarthy, E., Chow, E., Aran, D., Ilano, A., Pai, C.C.S., Rancan, C., et al. (2020). Intratumoral CD4+ T cells mediate anti-tumor cytotoxicity in human bladder cancer. *Cell* 181, 1612–1625.e13. <https://doi.org/10.1016/j.cell.2020.05.017>. <https://www.ncbi.nlm.nih.gov/pubmed/32497499>.
- Ott, P.A., Hu, Z., Keskin, D.B., Shukla, S.A., Sun, J., Bozym, D.J., Zhang, W., Luoma, A., Giobbie-Hurder, A., Peter, L., et al. (2017). An immunogenic personal neoantigen vaccine for patients with melanoma. *Nature* 547, 217–221. <https://doi.org/10.1038/nature22991>. <https://www.ncbi.nlm.nih.gov/pubmed/28678778>.
- Ott, P.A., Hu-Lieskovian, S., Chmielowski, B., Govindan, R., Naing, A., Bhardwaj, N., Margolin, K., Awad, M.M., Hellmann, M.D., Lin, J.J., et al. (2020). A phase ib trial of personalized neoantigen therapy plus anti-PD-1 in patients with advanced melanoma, non-small cell lung cancer, or bladder cancer. *Cell* 183, 347–362.e24. <https://doi.org/10.1016/j.cell.2020.08.053>. <https://www.ncbi.nlm.nih.gov/pubmed/33064988>.
- Patil, V.S., Madrigal, A., Schmiedel, B.J., Clarke, J., O'Rourke, P., de Silva, A.D., Harris, E., Peters, B., Seemois, G., Weiskopf, D., et al. (2018). Precursors of human CD4 + cytotoxic T lymphocytes identified by single-cell transcriptome analysis. *Sci. Immunol.* 3. <https://doi.org/10.1126/sciimmunol.aan8664>. <https://www.ncbi.nlm.nih.gov/pubmed/29352091>.
- Paz-Ares, L.G., Ramalingam, S.S., Ciuleanu, T.E., Lee, J.S., Urban, L., Caro, R.B., Park, K., Sakai, H., Ohe, Y., Nishio, M., et al. (2022). First-line nivolumab plus ipilimumab in advanced NSCLC: 4-year outcomes from the randomized, open-label, phase 3 CheckMate 227 Part 1 trial. *J. Thorac. Oncol.* 289–308. <https://doi.org/10.1016/j.jtho.2021.09.010>. <https://www.ncbi.nlm.nih.gov/pubmed/34648948>.
- Petitprez, F., de Reynies, A., Keung, E.Z., Chen, T.W.W., Sun, C.M., Calderaro, J., Jeng, Y.M., Hsiao, L.P., Lacroix, L., Bougouin, A., et al. (2020). B cells are associated with survival and immunotherapy response in sarcoma. *Nature* 577, 556–560. <https://doi.org/10.1038/s41586-019-1906-8>. <https://www.ncbi.nlm.nih.gov/pubmed/31942077>.
- Poran, A., Scherer, J., Bushway, M.E., Besada, R., Balogh, K.N., Wanamaker, A., Williams, R.G., Prabhakara, J., Ott, P.A., Hu-Lieskovian, S., et al. (2020). Combined TCR repertoire profiles and blood cell phenotypes predict melanoma patient response to personalized neoantigen therapy plus anti-PD-1. *Cell Rep. Med.* 1, 100141. <https://doi.org/10.1016/j.xcrm.2020.100141>. <https://www.ncbi.nlm.nih.gov/pubmed/33294862>.
- Powles, T., Assaf, Z.J., Davarpanah, N., Banchereau, R., Szabados, B.E., Yuen, K.C., Grivas, P., Hussain, M., Oudard, S., Gschwend, J.E., et al. (2021). ctDNA guiding adjuvant immunotherapy in urothelial carcinoma. *Nature* 595, 432–437. <https://doi.org/10.1038/s41586-021-03642-9>. <https://www.ncbi.nlm.nih.gov/pubmed/34135506>.
- Reck, M., Rodríguez-Abreu, D., Robinson, A.G., Hui, R., Csösz, T., Fülop, A., Gottfried, M., Peled, N., Tafreshi, A., Cuffe, S., et al. (2019). Updated analysis of KEYNOTE-024: pembrolizumab versus platinum-based chemotherapy for advanced non-small-cell lung cancer with PD-L1 tumor proportion score of 50% or greater. *J. Clin. Oncol.* 37, 537–546. <https://doi.org/10.1200/JCO.18.00149>. <https://www.ncbi.nlm.nih.gov/pubmed/30620668>.
- Reinert, T., Henriksen, T.V., Christensen, E., Sharma, S., Salari, R., Sethi, H., Knudsen, M., Nordentoft, I., Wu, H.T., Tin, A.S., et al. (2019). Analysis of

- plasma cell-free DNA by ultradeep sequencing in patients with stages I to III colorectal cancer. *JAMA Oncol.* 5, 1124–1131. <https://doi.org/10.1001/jamaonc.2019.0528>. <https://www.ncbi.nlm.nih.gov/pubmed/31070691>.
- Rimmer, A., Phan, H., Mathieson, I., Iqbal, Z., Wilkie, A.O.M., Consortium, W.G.S., Wilkie, A.O.M., McVean, G., and Lunter, G. (2014). Integrating mapping-assembly- and haplotype-based approaches for calling variants in clinical sequencing applications. *Nat. Genet.* 46, 912–918. <https://doi.org/10.1038/ng.3036>. <https://www.ncbi.nlm.nih.gov/pubmed/25017105>.
- Rizvi, N.A., Hellmann, M.D., Snyder, A., Kvistborg, P., Makarov, V., Havel, J.J., Lee, W., Yuan, J., Wong, P., Ho, T.S., et al. (2015). Mutational landscape determines sensitivity to PD-1 blockade in non-small cell lung cancer. *Science* 348, 124–128. <https://doi.org/10.1126/science.aaa1348>.
- Rodríguez-Abreu, D., Powell, S.F., Hochmair, M.J., Gadgeel, S., Esteban, E., Felip, E., Speranza, G., De Angelis, F., Dómíne, M., Cheng, S.Y., et al. (2021). Pemetrexed plus platinum with or without pembrolizumab in patients with previously untreated metastatic nonsquamous NSCLC: protocol-specified final analysis from KEYNOTE-189. *Ann. Oncol.* 32, 881–895. <https://doi.org/10.1016/j.annonc.2021.04.008>. <https://www.ncbi.nlm.nih.gov/pubmed/33894335>.
- Sahin, U., Derhovanessian, E., Miller, M., Kloke, B.P., Simon, P., Lower, M., Bukur, V., Tadmor, A.D., Luxemburger, U., Schrros, B., et al. (2017). Personalized RNA mutanome vaccines mobilize poly-specific therapeutic immunity against cancer. *Nature* 547, 222–226. <https://doi.org/10.1038/nature23003>. <https://www.ncbi.nlm.nih.gov/pubmed/28678784>.
- Saunders, C.T., Wong, W.S.W., Swamy, S., Becq, J., Murray, L.J., and Cheetham, R.K. (2012). Strelka: accurate somatic small-variant calling from sequenced tumor-normal sample pairs. *Bioinformatics* 28, 1811–1817. <https://doi.org/10.1093/bioinformatics/bts271>. <https://www.ncbi.nlm.nih.gov/pubmed/22581179>.
- Schneider, C.A., Rasband, W.S., and Eliceiri, K.W. (2012). NIH Image to ImageJ: 25 years of image analysis. *Nat. Methods* 9, 671–675.
- Signorell, A., Aho, K.A., Alfons, A., Anderegg, N., Aragon, T., Arppe, A., Baddeley, A., Barton, K., Bolker, B., Borchers, H.W., et al. (2016). DescTools: tools for descriptive statistics. <https://rdrr.io/cran/DescTools/man/DescToolspackage.html>.
- Snyder, A., Morrissey, M.P., and Hellmann, M.D. (2019). Use of circulating tumor DNA for cancer immunotherapy. *Clin. Cancer Res.* 25, 6909–6915. <https://doi.org/10.1158/1078-0432.CCR-18-2688>. <https://www.ncbi.nlm.nih.gov/pubmed/31285372>.
- Stuart, T., Butler, A., Hoffman, P., Hafemeister, C., Papalexi, E., Mauck, W.M., Hao, Y., Stoeckius, M., Smibert, P., and Satija, R. (2019). Comprehensive integration of single-cell data. *Cell* 177, 1888–1902.e21. <https://doi.org/10.1016/j.cell.2019.05.031>. <https://www.ncbi.nlm.nih.gov/pubmed/31178118>.
- Veatch, J.R., Jesernig, B.L., Kargl, J., Fitzgibbon, M., Lee, S.M., Baik, C., Martins, R., Houghton, A.M., and Riddell, S.R. (2019). Endogenous CD4+ T Cells Recognize Neoantigens in Lung Cancer Patients, Including Recurrent oncogenicKRAS and ERBB2 (Her2) driver mutationsEndogenous CD4+ T Cells Recognize Neoantigens in Lung Cancer Patients, Including Recurrent Oncogenic) Driver Mutations. *Cancer Immunol. Res.* 7, 910–922. <https://doi.org/10.1158/2326-6066.CIR-18-0402>. <https://www.ncbi.nlm.nih.gov/pubmed/31043415>.
- Wang, M., Herbst, R.S., and Boshoff, C. (2021). Toward personalized treatment approaches for non-small-cell lung cancer. *Nat. Med.* 27, 1345–1356. <https://doi.org/10.1038/s41591-021-01450-2>. <https://www.ncbi.nlm.nih.gov/pubmed/34385702>.
- Wickham, H. (2016). *ggplot2: Elegant Graphics for Data Analysis* (Springer-Verlag).
- Xu-Monette, Z.Y., Xiao, M., Au, Q., Padmanabhan, R., Xu, B., Hoe, N., Rodríguez-Perales, S., Torres-Ruiz, R., Manyam, G.C., Visco, C., et al. (2019). Immune profiling and quantitative analysis decipher the clinical role of immune-checkpoint expression in the tumor immune microenvironment of DLBCL. *Cancer Immunol. Res.* 7, 644–657. <https://doi.org/10.1158/2326-6066.CIR-18-0439>. <https://www.ncbi.nlm.nih.gov/pubmed/30745366>.

STAR★METHODS

KEY RESOURCES TABLE

| REAGENT or RESOURCE | SOURCE | IDENTIFIER |
|---|----------------|--------------------------------|
| Antibodies | | |
| Streptavidin R-PE | Agilent | Cat # PJRS25-1 |
| Streptavidin PE | Biolegend | Cat # 405204 |
| Streptavidin APC | Agilent | Cat # PJ27S |
| Streptavidin APC | Biolegend | Cat # 405207 |
| Streptavidin BV711 | BD Biosciences | Cat # 563262 |
| Streptavidin BV711 | BioLegend | Cat # 405241 |
| Streptavidin BV605 | BioLegend | Cat # 405229 |
| Streptavidin PE-CF594 | BD Biosciences | Cat # 562284 |
| Streptavidin BV421 | Biolegend | Cat # 405225 |
| Streptavidin BUV395 | BD Biosciences | Cat # 564176 |
| Streptavidin BV650 | BD Biosciences | Cat # 563855 |
| Streptavidin BV650 | BioLegend | Cat # 405232 |
| LIVE/DEAD Fixable Near-IR Dead Cell Stain Kit | ThermoFisher | Cat # L10119 |
| CD19 APC-H7 | BD Biosciences | Cat # 560177; RRID:AB_1645470 |
| CD3 BUV805 | BD Biosciences | Cat # 612893; RRID:AB_2870181 |
| CD3 APC | BD Biosciences | Cat # 340661 |
| CD3 BV711 | BD Biosciences | Cat # 740832; RRID:AB_2740489 |
| CD4 BV711 | BD Biosciences | Cat # 563028; RRID:AB_2737961 |
| CD4 BUV395 | BD Biosciences | Cat # 563028 |
| CD4 FITC | Biolegend | Cat # 300306 |
| CD8 Alexa Fluor 700 | BD Biosciences | Cat # 561423; RRID:AB_10682894 |
| CD8 APC-H7 | BD Biosciences | Cat # 563795; RRID:AB_2722501 |
| CD8 BUV395 | BD Biosciences | Cat # 555636; RRID:AB_395998 |
| CD8 PE-Cy5 | BD Biosciences | Cat # 563561; RRID:AB_2744288 |
| CD14 BUV395 | BD Biosciences | Cat # 563785; RRID:AB_2744293 |
| CD16 BUV395 | BD Biosciences | Cat # 560177; RRID:AB_1645470 |
| CD19 APC-H7 | BD Biosciences | Cat # 563549; RRID:AB_2738272 |
| CD19 BUV395 | BD Biosciences | Cat # 564655; RRID:AB_2744311 |
| CD19 BUV496 | BD Biosciences | Cat # 562661; RRID:AB_2744343 |
| CD25 BV605 | BD Biosciences | Cat # 302710; RRID:AB_10916120 |
| CD26 APC | Biolegend | Cat # 557745; RRID:AB_396851 |
| CD69 PE-Cy7 | BD Biosciences | Cat # 555543; RRID:AB_395927 |
| CD62L FITC | BD Biosciences | Cat # 560607; RRID:AB_1727500 |
| CD45RO | BD Biosciences | Cat # 560673; RRID:AB_1727496 |
| CD45RA Alexa Fluor 700 | BD Biosciences | Cat # 561423; RRID:AB_10682894 |
| CD107a BV786 | BD Biosciences | Cat # 563869; RRID:AB_2738458 |
| CD137 (41BB) BV650 | BD Biosciences | Cat # 564092; RRID:AB_2738586 |
| CD152 (CTLA4) BV421 | BD Biosciences | Cat # 562743; RRID:AB_2737762 |
| CD152 (CTLA4) PE-Cy5 | BD Biosciences | Cat # 555854; RRID:AB_396177 |
| CD223 (Lag3) BUV605 | BD Biosciences | Cat # 745160; RRID:AB_2742761 |
| CD223 (Lag3) BV786 | BD Biosciences | Cat # 744727; RRID:AB_2742438 |
| CD278 (ICOS) BUV395 | BD Biosciences | Cat # 564777; RRID:AB_2738946 |
| CD278 (ICOS) BV421 | BD Biosciences | Cat # 562901; RRID:AB_2737878 |

(Continued on next page)

Continued

| REAGENT or RESOURCE | SOURCE | IDENTIFIER |
|--|------------------------|-----------------------------------|
| CD366 (Tim3) BV510 | Biolegend | Cat # 345030; RRID:AB_2565831 |
| Foxp3 PE-Cy7 | Thermo Fisher | Cat # 25-4776-42 |
| HLA-DR BUV496 | BD Biosciences | Cat # 749866; RRID:AB_2874106 |
| IFN γ PE | Thermo Fisher | Cat # 61-2799-42; RRID:AB_2574598 |
| PD-1 PE-eFluor 610 | eBioscience | Cat # 328649; RRID:AB_2800854 |
| TotalSeq™-C0155 anti-human CD107a (LAMP-1) | BioLegend | Cat # 353251; RRID:AB_2800943 |
| TotalSeq™-C0155 anti-human CD197 (CCR7) | BioLegend | Cat # 302649; RRID:AB_2800745 |
| TotalSeq™-C0155 anti-human CD25 | BioLegend | Cat # 302853; RRID:AB_2800747 |
| TotalSeq™-C0155 anti-human CD27 | BioLegend | Cat # 313553 |
| TotalSeq™-C0155 anti-human CD278 (ICOS) | BioLegend | Cat # 328237; RRID:AB_2800853 |
| TotalSeq™-C0155 anti-human CD39 | BioLegend | Cat # 304163; RRID:AB_2800764 |
| TotalSeq™-C0155 anti-human CD45RA | BioLegend | Cat # 304259; RRID:AB_2800766 |
| TotalSeq™-C0155 anti-human CD45RO | BioLegend | Cat # 304851; RRID:AB_2800770 |
| TotalSeq™-C0155 anti-human CD62L | BioLegend | Cat # 351356; RRID:AB_2800937 |
| TotalSeq™-C0155 anti-human CD127 (IL-7R α) | BioLegend | Cat # 309839; RRID:AB_2800807 |
| TotalSeq™-C0155 anti-human CD137 (4-1BB) | BioLegend | Cat # 369621; RRID:AB_2801015 |
| TotalSeq™-C0155 anti-human CD152 (CTLA-4) | BioLegend | Cat # 369335; RRID:AB_2814327 |
| TotalSeq™-C0155 anti-human CD223 (LAG-3) | BioLegend | Cat # 302722; RRID:AB_2810435 |
| TotalSeq™-C0155 anti-human CD26 | BioLegend | Cat # 329963; RRID:AB_2800862 |
| TotalSeq™-C0155 anti-human CD279 (PD-1) | BioLegend | Cat # 345049; RRID:AB_2800925 |
| TotalSeq™-C0155 anti-human CD366 (Tim-3) | BioLegend | Cat # 310951; RRID:AB_2800810 |
| TotalSeq™-C0155 anti-human CD69 | BioLegend | Cat # 372729; RRID:AB_2801021 |
| TotalSeq™-C0155 anti-human TIG IT (VSTM3) | BioLegend | Cat # 61-2799-42; RRID:AB_2574598 |
| TotalSeq™-C0155 anti-human KLRG1 (MAFA) | BioLegend | Cat # 138433 |
| CD3 | Thermo Fisher | Cat # MA1-90582 |
| CD4 | Abcam | Cat # ab133616; RRID:AB_2750883 |
| HLA DP/DQ/DR | Thermo Fisher | Cat # MA1-25914 |
| Pan CK | Biocare | Cat # CM011A |
| DAPI | Fisher Scientific | Cat # D21490 |
| CD3 [F7.2.38] | Dako | Cat # M7254; RRID:AB_2631163 |
| CD4 [EPR6855] | Abcam | Cat # ab181724; RRID:AB_2864377 |
| CD8 [C8/144B] | Dako | Cat # M7103; RRID:AB_2075537 |
| Cytokeratin [PCK-26] | Sigma Aldrich | Cat # C5992; RRID:AB_2134432 |
| Cytokeratin [AE1] | eBioscience | Cat # 14-9001-82; RRID:AB_1834477 |
| Biological samples | | |
| Patient PBMCs from NT-002 trial | This manuscript | N/A |
| Patient Tumor Biopsies from NT-002 trial | This manuscript | N/A |
| Healthy Donor PBMCs | Precision for Medicine | Cat # 93000-10M |
| Healthy Donor PBMCs | StemExpress | Cat # LE010F |

(Continued on next page)

Continued

| REAGENT or RESOURCE | SOURCE | IDENTIFIER |
|--|----------------------|-------------------|
| Chemicals, peptides, and recombinant proteins | | |
| CEF viral peptide pool | JPT | Cat # PM-CEF-E |
| Cell Stimulation Cocktail | Life Technologies | Cat # 00-4970-93 |
| Dasatinib | Sigma-Aldrich | Cat # CDS023389 |
| Benzonase | Millipore Sigma | Cat # 70746 |
| d-biotin solution | AVIDITY | Cat # BIO200 |
| MHC class II tetramers | This manuscript | N/A |
| Critical commercial assays | | |
| 5 Feature Barcode kit | 10X Genomics | Cat # 1000256 |
| Chromium Next GEM ChipK single cell kit | 10X Genomics | Cat # 1000286 |
| Chromium Next GEM Single Cell 5 Kit v2 | 10X Genomics | Cat # 1000263 |
| Chromium Single Cell Human TCR Amplification Kit | 10X Genomics | Cat # 1000252 |
| Library Construction Kit | 10X Genomics | Cat # 1000190 |
| Dual Index Kit TN Set A | 10X Genomics | Cat # 1000250 |
| Dual Index Kit TT Set A | 10X Genomics | Cat # 1000215 |
| MiSeq Reagent Kit v2 (300 cycles) | Illumina | Cat # MS-102-2002 |
| Agilent HS DNA kit | Agilent Technologies | Cat # 5067-4626 |
| Pan T cell isolation kit | Miltenyi Biotec | Cat # 130-096-535 |
| AEC substrate-chromogen | BD Biosciences | Cat # 551951 |
| Fixation/Permeabilization Solution Kit | BD Biosciences | Cat # 554714 |
| Foxp3/Transcription Factor Staining Buffer Set | eBioscience | Cat # 00-5523-00 |
| Intracellular Fixation and Permeabilization Buffer Set | eBioscience | Cat # 88-8824-00 |
| GolgiStop | BD Biosciences | Cat # 554724 |
| GolgiPlug | BD Biosciences | Cat # 555029 |
| IFN gamma Human ELISPOT Kit | Invitrogen | Cat # 88-7386-88 |
| U-Plex development pack, 10-assay sector plate | Meso Scale Discovery | Cat # K15235N |
| Meso Scale Discovery (MSD) Read Buffer T (4x) | Meso Scale Discovery | Cat # R92TC |
| Meso Scale Discovery (MSD) U-Plex System | Meso Scale Discovery | Cat # K15067L |
| CD3 MicroBeads, human | Miltenyi Biotec | Cat # 130-050-101 |
| CD4 MicroBeads, human | Miltenyi Biotec | Cat # 130-045-101 |
| AllPrep DNA/RNA FFPE kit | Qiagen | Cat # 80234 |
| Qubit RNA HS Assay Kit | ThermoFisher | Cat # Q32855 |
| RNA 6000 Nano Kit | Agilent | Cat # 5067-1511 |
| RNA 6000 Pico Kit | Agilent | Cat # 5067-1513 |
| RNeasy Plus Micro Kit | Qiagen | Cat # 74034 |
| RNeasy Plus Mini Kit | Qiagen | Cat # 74134 |
| Prolong Gold | Fisher Scientific | Cat # P36930 |
| OPAL 540 | Akoya | Cat # FP1494001KT |
| OPAL 620 | Akoya | Cat # FP1495001KT |
| OPAL 650 | Akoya | Cat # FP1496001KT |
| OPAL 690 | Akoya | Cat # FP1497001KT |
| ImmPRESS Universal HRP | Vector | Cat # MP-7800 |
| Antibody diluent/block | Akoya | Cat # ARD1001EA |
| Antigen unmasking solution, citrate based | Vector labs | Cat # H-3300 |

(Continued on next page)

Continued

| REAGENT or RESOURCE | SOURCE | IDENTIFIER |
|--|--|---|
| Antigen unmasking solution, tris based | Vector labs | Cat # H-3301 |
| Experimental models: Cell lines | | |
| Jurkat, Clone E6-1 | ATCC | Cat # ATCC-TIB-152 |
| 293FT Cell Line | Thermo Fisher | Cat # R70007 |
| FuGENE® HD Transfection Reagent | Promega Corporation | Cat # E2311 |
| Software and algorithms | | |
| R (version 4.0.5) | CRAN | https://www.r-project.org/ |
| Image J (version 1.53n) | Schneider et al., 2012 | https://imagej.nih.gov/ij/ |
| FlowJo (version 10) | FlowJo™ Software (for Windows) Version 10. Becton, Dickinson and Company; 2019. | https://www.flowjo.com/ |
| IPD-IMGT/HLA | N/A | https://www.ebi.ac.uk/ipd/imgt/hla |
| GraphPad Prism (version 9) | GraphPad Software, La Jolla California, USA | www.graphpad.com |
| BWA-MEM (version 0.7.13) | Li and Durbin, 2009 | N/A |
| STAR-Fusion (version 2.5.1.b) | Haas et al., 2017 | N/A |
| GATK 3.5 workflow | McKenna et al., 2010 | N/A |
| ConTest | Cibulskis et al., 2011 | N/A |
| VarDict (version 1.4.6) | Lai et al., 2016 | N/A |
| Strelka (version 1.0.15) | Saunders et al., 2012 | N/A |
| VarScan2 (version 2.3.9) | Koboldt et al., 2012 | N/A |
| Atlas Indel2 (version 1.4.3) | Challis et al., 2012 | N/A |
| Seurat (version 4.0.5) | Christoforides et al., 2013 | N/A |
| Platypus (version 0.8.1) | Rimmer et al., 2014 | N/A |
| RSEM (version 1.2.31) | Li and Dewey, 2011 | N/A |
| NetMHCpan (version 3.0) | Nielsen and Andreatta, 2016 | N/A |
| MIXCR (version 3.0.12) | Bolotin et al., 2015 | N/A |
| DescTools package | Signorell, 2016 | N/A |
| Loupe VDJ Browser (version 4.0) | 10x Genomics | N/A |
| SnapGene | SnapGene | N/A |

RESOURCE AVAILABILITY**Lead contact**

Further information and requests for resources and reagents should be directed to and will be fulfilled by the Lead Contact, Lakshmi Srinivasan (lakshmi.srinivasan@external.biotech.us).

Materials availability

All unique/stable reagents generated in this study are available from the [Lead contact](#) with a completed Materials Transfer Agreement.

Data and code availability

All vaccine peptide and immune assay peptide sequences are provided in [Table S6](#). Patient sequencing information will be provided upon request for patients consistent with their institutional informed consent. Epitope selection utilized previously published algorithms and methods as described in the [STAR Methods](#) (Ott et al., 2020).

EXPERIMENTAL MODEL AND SUBJECT DETAILS**NT-002 study design**

Details of the study can be found in the attached clinical study protocol NT-002 ([Data S1](#)) and patient demographics can be found in [Table 1](#).

The clinical sites that enrolled patients were Dana Farber Cancer Institute, Sarah Cannon Research Institute, University of California Los Angeles, and Washington University. Study protocol was reviewed and approved by institutional review boards and an informed consent was obtained from the patients enrolled in the study.

The primary objective of this phase 1b trial was to evaluate the safety of administering NEO-PV-01 with pembrolizumab/chemotherapy in untreated patients with advanced or metastatic non-squamous NSCLC. Secondary objectives included determination of anti-tumor activity, assessed by RECIST objective response rate, clinical benefit rate, duration of response, response conversion rate, progression free survival, and overall survival.

The study employed multiple exploratory objectives to characterize immune responses to NEO-PV-01 regimen in this population. Vaccine-induced responses were evaluated by assessment of antigen-specific CD8⁺ and CD4⁺ T cell responses in peripheral blood during and following vaccine administration. Correlation of patient responses including prolonged PFS with biomarkers in peripheral blood and tumor was conducted as an exploratory objective; assessments included tumor programmed death ligand (PD-L1) expression and abundance and phenotypes of tumor infiltrating lymphocytes. Patients samples used across the various assays are listed in [Table S6](#).

Treatment regimen

NEO-PV-01 is a personalized cancer vaccine consisting of up to 20 synthesized peptides of approximately 14–35 amino acids in length that are derived from an individual patient's mutated tumor DNA. The NEO-PV-01 drug product is administered following mixing with adjuvant poly-ICLC. For each patient, the peptides in poly-ICLC are divided in up to 4 pools for injection subcutaneously, rotating in extremity or flank site administrations.

In this phase 1b study, NEO-PV-01 therapy is administered following four 3-weekly cycles of a chemotherapy + pembrolizumab treatment regimen. Pembrolizumab was administered as a 200 mg IV infusion on cycle day 1 every 3 weeks. Carboplatin (AUC 5) and pemetrexed 500 mg/m² were also given on day 1 of each treatment cycle. Patients were required to receive all 4 pembrolizumab + chemotherapy cycles prior to vaccination. In instances where these treatments were held, NEO-PV-01 initiation was also delayed until all 4 cycles were complete.

All patients underwent radiographic evaluation at study week 8 to assess disease response to initial chemotherapy + pembrolizumab and had a confirmatory assessment at week 12 to document disease status prior to initiation of NEO-PV-01 vaccination.

NEO-PV-01 is administered on a schedule of 5 priming doses days 1 and 4 of study week 12 and then weekly in study weeks 13, 14, and 15. Two additional NEO-PV-01 administrations are provided as booster dosing on study weeks 19 and 23 to complete vaccine administration and the study primary treatment phase.

Pembrolizumab treatment was maintained on its every 3 week schedule during the week 12–24 vaccination period and then from weeks 24 –103 in the absence of progressive disease, initiation of an alternate antineoplastic therapy, intolerable toxicities, withdrawal of consent, or death.

Eligibility

Patients eligible for study participation were those with histologically confirmed, locally advanced or metastatic non-squamous NSCLC and no prior therapy for their advanced disease. Other key inclusion criteria include written informed consent for study participation, age \geq 18 years, ECOG performance status 0 or 1, at least 1 site of RECIST measurable disease, disease accessible for on treatment tumor biopsy, and acceptable screening laboratory values within 30 days prior to treatment including hematology: absolute neutrophil count (ANC) \geq 1.5 \times 10³/mL, platelet count \geq 100 \times 10³/mL, hemoglobin > 9 g/dL, chemistry: serum creatinine \leq 1.5 \times upper limit of normal (ULN) or creatinine clearance (CrCl) \geq 40 mL/min/1.73 m², aspartate aminotransferase (AST) and alanine aminotransferase (ALT) \leq 2.5 \times ULN or \leq 5 \times ULN with liver metastases, total bilirubin \leq 1.5 \times ULN or direct bilirubin \leq ULN for patients with total bilirubin levels > 1.5 \times ULN, and PT, PTT both < 1.5 \times ULN unless on anticoagulation therapy.

Patients eligible for study participation did not meet any of the following major exclusion criteria, including receipt of any prior systemic cancer therapy for advanced or metastatic NSCLC, receipt of any investigational agent or study therapy within 4 weeks of first study treatment, receipt of radiation therapy to the lung greater than 30 Gray < 6 months prior to study treatment, known CNS metastases unless clinically stable > 4 weeks, receipt of non-oncology vaccine therapy during and up to 8 weeks following the period of NEO-PV-01 administration, active autoimmune disease requiring systemic treatment within the last 2 years except for physiologic corticosteroid replacement therapy, interstitial lung disease, active pneumonitis or history of pneumonitis requiring corticosteroid therapy, unstable angina or congestive heart failure, active infection requiring treatment, active hepatitis B, C, or history of HIV, or history of invasive malignancy unless disease free > 2 years. Patients with anaplastic lymphoma kinase (ALK) translocations or epidermal growth factor receptor (EGFR) mutations must have received prior treatment with ALK or EGFR inhibitors, respectively.

A complete list of inclusion and exclusion criteria is provided in the NT-002 study protocol (Appendix).

Clinical assessments

Safety assessments conducted during the primary treatment phase included adverse event collection through patient reported symptoms, symptom-directed physical examination, and vital sign and safety laboratory assessments. Adverse events were monitored throughout the study from time of first dose of pembrolizumab (Cycle 1, Day 1) through study week 103 or 30 days after the last pembrolizumab treatment, whichever occurred first. Serious adverse events (SAEs) were reported from the time of signing the patient informed consent through study week 103 or 90 days after the last dose of pembrolizumab, whichever occurred first.

Radiographic assessments to evaluate response to study treatment were conducted at weeks 8 and 12 prior to NEO-PV-01 administration, at study weeks 24, 36, 51, 63, 75, 87, and 99. Anti-tumor activity was assessed for objective response rate (ORR), duration of response (DOR), progression free survival (PFS) and overall survival (OS). ORR is defined as the proportion of patients who achieve CR or PR based on RECIST v1.1. DOR is defined as the date of the first documented confirmed response to the date of the first documented PD or death. PFS is defined as the time from the date of first dosing to the date of first documented PD or death. OS is defined from the date of first dosing to death. Statistical efficacy analyses were performed for both the ITT set defined as receiving at least one dose of any study drug, and the safety set defined as receiving at least one dose of vaccine. The Kaplan–Meier method was used to estimate PFS and OS. For PFS, patients who did not have a PFS event on study or who missed 2 consecutive tumor assessments were censored at the time of next scheduled assessment from the last tumor assessment. For OS, patients who were alive or who were lost to follow-up were censored at the last record on database.

Patient samples

Patient samples collected on the study and analyzed across the various assays are listed in [Table S6](#). 38 patients were enrolled on the study. Peripheral blood mononuclear cells (PBMCs) samples for comprehensive immune system monitoring were obtained from leukaphereses performed up to 7 days prior to initiation of NEO-PV-01 vaccination, 7 days (Week 20) following the first NEO-PV-01 booster vaccination and then at study week 52. Additional immune monitoring assessments were performed from 80 mL peripheral blood samples obtained prior to study treatment, and study weeks 6, 14, 16, 24, 36, 48, 63, 75, 87, and 99. Patient PBMCs were processed and stored as described previously ([Ott et al., 2020](#)).

Tumor samples (surgical and core-needle biopsies) were obtained at pre-treatment, pre-vaccine (week 10–12) and post-vaccine (week 24) timepoints. Samples were processed and sequenced as described previously ([Ott et al., 2020](#)). Pre-treatment biopsies were used for generation of NEO-PV-01, and advanced for sequencing as described previously ([Ott et al., 2020](#)).

METHOD DETAILS

Generation of NEO-PV-01

Whole exome sequencing

As previously described ([Ott et al., 2020](#)), WES (library protocol: ACE(TM) Cancer Research Exome, Personalis, Menlo Park, CA) and RNA-Seq (library protocol: ACE(TM) Cancer Research Transcriptome, Personalis, Menlo Park, CA) libraries were sequenced using Illumina HiSeq in a CLIA/CAP accredited laboratory (Personalis, Menlo Park, CA). WES was conducted on a tumor sample and a normal blood sample per patient (depths: 163–335 reads and 80–137 reads, respectively); RNA-Seq was conducted on tumor samples only (depth: 37–309 reads).

The HLA-A, HLA-B, and HLA-C genotype of each patient was determined by amplifying informative exons by polymerase chain reaction (PCR) using locus-specific primers. Dye-terminator sequencing fragments from the PCR fragments were analyzed on a capillary sequencer to determine nucleotide sequences for each haplotype (BloodCenter of Wisconsin, Milwaukee, WI).

Alignment and mutation calling

All alignment, mutation calling and filtering, and gene expression quantification was done in accordance with methods described previously ([Ott et al., 2020](#)). In the event that an adequate RNA library could not be prepared, methods described previously were implemented ([Ott et al., 2020](#)). All computational analysis steps were conducted using an automated analysis pipeline hosted on a cloud computing platform (Seven Bridges Genomics, Charlestown, MA). Tumor and germline WES and tumor RNA-Seq FASTQs were aligned to the human genome (Gencode V19) using the BWA-MEM (version 0.7.13) (H. Li and Durbin 2009) and STAR (version 2.5.1.b), respectively. All alignments were post-processed with the GATK 3.5 workflow ([McKenna et al., 2010](#)) including GATK Indel Realigner, GATK Base Recalibrator, and Picard Mark Duplicates (version 1.140). ConTest ([Cibulskis et al., 2011](#)) was used to confirm that all three samples originated from the same individual. Somatic variants were called on the basis of tumor and normal WES using an ensemble of seven different mutation calling algorithms: VarDict (version 1.4.6) ([Lai et al., 2016](#)), Strelka (version 1.0.15) ([Saunders et al., 2012](#)), VarScan2 (version 2.3.9) ([Koboldt et al., 2012](#)), Mutect2 (from the GATK version 3.5 bundle) ([Cibulskis et al., 2011](#)), Atlas Indel2 (version 1.4.3) ([Challis et al., 2012](#)), Seurat (version 2.6) ([Christoforides et al., 2013](#)), and Platypus (version 0.8.1) ([Rimmer et al., 2014](#)). The three sequencing datasets were then realigned using HaplotypeCaller (from the GATK version 3.5 bundle), specifying the candidate mutations (union of the seven call sets) as known variants. Finally, the variants were filtered according to the following features: the level of read support in the tumor WES data, the presence of variant reads in the normal WES data, read orientation bias, adequacy of coverage in the normal WES sample, the presence of neighboring (+/-30nt) variants (somatic or germline), and read quality bias observed in mutation-supporting reads. RNA-Seq expression levels of all genes and transcripts were quantified in transcripts per million (TPM) using RSEM (version 1.2.31) (B. Li and Dewey 2011). The overall expression of each somatic variant was calculated as the product of the RSEM-derived transcript expression (summing across all overlapping protein-coding transcripts) and the fraction of RNA-Seq reads supporting the variant. Variants with zero supporting RNA reads were still considered as valid mutations (and counted toward tumor mutation burden) but were not considered for inclusion in vaccine. RNA-Seq was additionally processed using STAR-Fusion (version 2.5.1.b) to identify transcript fusions (requiring both junction support and spanning read pairs). In the event that an adequate RNA library could not be prepared, fusion calling was skipped, and reference expression was obtained from TCGA samples with high tumor purity (as assessed by Absolute; five samples per tumor type) ([Carter et al. 2012](#)). Since these patients lacked RNA-Seq as a filter against false positive

mutation calls, their somatic variants were required to have a higher level of read support in the tumor WES and to have been identified by more than one mutation caller.

Vaccine peptide selection

Patients with at least 50 non-synonymous point mutations and/or gene fusions were advanced to the vaccine design step. The vaccine peptides, also referred to as immunizing (IM) peptides, were identified by selecting 6 peptides on the basis of HLA-I presentation scores (also referred to as epitope quality scores, see below), 2 peptides based on high expression, and 2 peptides based on highly expressed frameshifts, iteratively until the full roster of 30 peptides was completed. The latter two epitope classes were required to have expression levels > 10 TPM and > 5 TPM, respectively (if none were available, the slots were ceded to HLA-I selections). Generally, each mutation was targeted by only one vaccine peptide and excluded from subsequent selections unless the span of novel sequence generated could not be covered by a single peptide (as can happen with frameshifts) or if the likelihood of manufacturing success was questionable for the first peptide per known synthesis constraints. The trade-off between synthesis constraints and immune-related scoring further dictated the relative length of the vaccine peptides (allowable range: 14–35 amino acids) and whether they were centered or shifted with respect to the site of mutation.

HLA-I presentation scores were determined based on a logistic regression that considered binding predictions, allele-specific expression, and proteasomal cleavage potential. Binding predictions were calculated as the weighted average of NetMHCpan-3.0 percent rank (Nielsen and Andreatta 2016) and a neural network trained on mass spectrometry data using methods described previously (Abelin et al. 2017) with respective weights of 20% and 80%. Proteasomal cleavage potential was also calculated using a neural network trained on mass spectrometry data using methods described previously (Abelin et al. 2017). The score of a candidate vaccine peptide was determined by summing all the relevant peptide-allele combinations (epitopes lengths 8–12; HLA-A HLA-B, and HLA-C alleles).

Secondary characteristics were used to up-weight and down-weight candidate epitopes but were purposely tuned to have less importance than the above-mentioned factors. Thus, all other parameters being equal, the selection algorithm favored more clonal epitopes (higher mutant allele fraction) over sub-clonal epitopes, frameshifts over point mutations, oncogenes over passenger genes, and peptides with good manufacturing scores over those with poor predicted manufacturability. Our scoring system did not consider the relative binding scores of wild-type peptides or similarity to known pathogen sequences (Luksza et al. 2017).

GMP peptide manufacturing

The GMP grade peptides of NEO-PV-01 were manufactured as described previously (Ott et al., 2020). The GMP grade peptides of NEO-PV-01 were synthesized using solid-phase peptide synthesis (SPPS) on automated parallel peptide synthesizers. 9-fluorenylmethyloxycarbonyl (Fmoc) chemistry was employed. After the assembly of the peptide chains, the peptides were removed from the resins using cleavage cocktails containing trifluoroacetic acid and scavengers. The peptides were precipitated and washed with ether. After drying, the crude peptides were purified on automated preparative high-performance liquid chromatography (prep HPLC) systems with UV and mass spectrometry (MS) detectors. The prep HPLC fractions were analyzed using ultra-performance liquid chromatography (UPLC)-UV/MS systems to determine molecular weights (MW) and purities. The fractions containing the target peptides and desired purities were lyophilized to solid powders with the final purities equal to or higher than 95%. Up to 20 peptides per vaccine were formulated in a buffered aqueous solution containing 4% DMSO in isotonic dextrose and mixed into up to four pools, each containing up to five peptides. The pooled peptide solutions were filtered through 0.22 mm filters for sterilization. The vaccines were analyzed for identity (molecular weights based on UPLC-UV/MS analysis), sterility, endotoxin, and strength before their releases from the GMP manufacturing site. The amino- and carboxyl-termini of the peptides are free amines and carboxylic acids respectively, without structural modifications.

Peptide synthesis for immunological assays

The peptides for *in vitro* immune response studies, immune assay peptides (IAP) were synthesized using SPPS on computer-controlled high-throughput peptide synthesizers. The peptides were assembled on resins by employing Fmoc chemistry. The chemical cleavages of peptides from the resins were performed by using TFA solution containing scavengers followed by peptide precipitation and washes with diethyl ether. The assay peptides (ASP) were purified on automated prep HPLC systems equipped with UV and MS detectors. The prep HPLC fractions of each peptide that met the molecular weight (MW) and purity criteria based on UPLC-UV/MS analysis were pooled and dried using either parallel centrifugal evaporators or lyophilizers. The epitope peptides (EPT) were resuspended in acetonitrile and water and dried on a lyophilizer after diethyl ether washes and analyzed for required purity and MW by using UPLC-UV/MS. Assay peptides (ASP) were 13–15 amino acids and overlapped by at least 9 amino acids to cover the immunizing peptide (IM) sequence or were 8–11 amino acids and predicted to bind class I (Ott et al., 2017). All peptide sequences are provided in Table S6.

Personalized ctDNA assays

Design and application of personalized and tumor-informed ctDNA (multiplex-PCR, next-generation sequencing) assays was conducted with blinding to clinical data by Natera. Paired tumor and peripheral blood WES data were used to identify and design the Signatera assay with 16 tumor-specific somatic single nucleotide variants (SNVs) for each patient. Additionally, another custom assay consisting of 16 tumor-specific SNVs was designed from our BioNTech's list of 30 prioritized high-quality patient-specific neoepitopes based on designability and other internal bioinformatics algorithmic criteria (Reinert et al., 2019; Coombes et al., 2019; Christensen et al., 2019). Given that these algorithms were developed independently, there is a potential of variants to overlap between the two assays. For the

first Signatera 16-plex assay, SNVs present in the tumor but absent in the germline were used to select the 16 targets, with prioritization based on multiple factors, including the observed variant allele frequency in the tumor tissue and the associated background noise profile in the plasma. The multiplexed targeted PCR was conducted followed by amplicon deep sequencing on an Illumina platform. Variant allele frequencies were determined for each of the target mutations. The plasma sample was considered ctDNA-positive on observing at least two or more variants. Absolute ctDNA levels were then calculated for ctDNA-positive plasma samples (MTM per mL) by normalizing variant allele frequencies observed by the plasma volume used for each sample. As described previously, MTM per mL was calculated from all tested targets, including undetected targets (Bratman et al., 2020).

Detection of neoantigen-specific immune responses

Neoantigen-specific immune responses were detected either *ex vivo* or after 5-day stimulation as described previously (Ott et al., 2020). For *ex vivo* assays, patient PBMCs were rested overnight at 2×10^6 cells/mL in X-Vivo media (Lonza) supplemented with 1% penicillin/streptomycin (GIBCO). For neoantigen pre-exposure assays, patient PBMCs were rested overnight and cultured with individual peptides (2mM) or pooled peptides (2mM per peptide) for 5 days at a density of 5×10^6 cells/ml in a 24-well plate. On day 3 of culture, half the well volume was replaced with fresh media. All immunizing peptides were tested in both the *ex vivo* as well as in the 5-day stimulation with the neoantigen peptide assay formats. Immunizing peptides are referred to as IM followed by the peptide number.

IFN γ ELISpot assay

IFN- γ ELISpots were performed as described previously (Ott et al., 2020). IFN γ ELISpot assays were performed using 96-well Multi-Screen Filter Plates (Millipore) and the Ready-Set-Go! Human IFN γ ELISpot Kit (Invitrogen) according to manufacturer's instructions. Plates were coated overnight at 4 °C with anti IFN γ Capture Antibody diluted in 1X Coating Buffer, washed with 1X Coating Buffer and blocked with X Vivo media (Lonza) containing 1% penicillin/streptomycin (GIBCO) for 1h. For *ex vivo* ELISpots, PBMCs were plated in triplicate with 1×10^6 cells per well. For cells that were pre-exposed to peptide, cells were washed and plated in triplicate with 1×10^5 cells per well. Peptides were added to ELISpot wells at 2mM per peptide. Each plate included a healthy donor positive and negative control with the CEF viral peptide pool (JPT) and Cell Stimulation Cocktail (Life Technologies) to confirm reagent performance. Plates were incubated overnight at 37 °C. Plates were washed 3 times using PBS with 0.05% Tween 20 and detection antibody diluted in 1X ELISpot diluent was added to wells for 2h. After washing 3 times with PBS with 0.05% Tween 20, Avidin-HRP was diluted in 1X ELISpot diluent and added to wells for 45 min. Plates were washed with both PBS with Tween 20 and PBS 3 times. AEC substrate-chromogen (BD Biosciences) was then added for 20 min. Plates were rinsed with deionized water 3 times and allowed to dry at room temperature overnight. Spots were imaged and enumerated using an Immunospot analyzer (Cellular Technology Limited). Responses were characterized as positive if spot-forming cell count detected was at least 10 spots over the DMSO control and +3 standard deviations and confirmed in repeat experiments.

Characterization of CD4 $^+$ /CD8 $^+$ T cell responses

CD4 $^+$ and CD8 $^+$ T cell response were characterized as described previously (Ott et al., 2020). CD3 $^+$ T cells were isolated from patient PBMCs by negative selection using the Pan T cell isolation kit (Miltenyi). Both the CD3 $^+$ and CD3 $^-$ populations were collected, washed, and counted after isolation. The CD3 $^-$ population was used as APCs (antigen-presenting cells) for this assay. The CD3 $^+$ population then underwent CD4 $^+$ positive isolation using CD4 $^+$ microbeads (Miltenyi). Both the CD4 $^+$ (positive-selection) and CD8 $^+$ (negative-selection) T cells were collected, washed, and counted. A co-culture containing APCs and either CD4 $^+$ or CD8 $^+$ cells at a ratio of 3:1, 2:1, or 1:1 were plated in a 96-well flat bottom polystyrene plate for 24–48h. Peptide was added directly to wells, in triplicate, at 2mM per peptide. If the T cells were pre-exposed to neoantigen peptide for 5–6 days, CD3 $^-$ APCs were isolated from fresh patient PBMCs using CD3 microbeads (Miltenyi). Supernatants were collected at the end of the co-culture and frozen at –80 °C until use. The Meso Scale Discovery (MSD) U-Plex system was used to detect 10 distinct analytes from the co-culture supernatants. The analytes measured were: IL-1 β , IL-2, IL-6, IL-9, IL-13, IL-15, IL-17a, IFN γ , and TNF- α . MSD 10-plex plates were coated with the linker-antibody solution for 1h with shaking at room temperature. The plates were then washed 3 times with PBS with 0.05% Tween 20 on a BioTek plate washer. Supernatant and standards were diluted 1:2 and added to the plate for 1h with shaking at room temperature. Plates were washed again with PBS with 0.05% Tween 20 before the addition of the detection antibody solution for 1h. Plates were washed with PBS with 0.05% Tween 20 and 2X Read Buffer (MSD) was added to the plates for detection on the MSD SECTOR S 600 instrument. Concentration in pg/mL was calculated by the MSD Discovery Workbench software by comparing luminescent signal of the patient samples against the known standard curve. CD4 $^+$ and CD8 $^+$ positive responses were determined separately based on the corresponding DMSO controls. A positive signal was determined by an IFN γ signal 1.5-fold higher than the DMSO control.

CD107a mobilization assay

Detection of CD107a mobilization on both CD4 $^+$ and CD8 $^+$ T cells was performed using flow cytometry as described previously in (Ott et al., 2020). For *ex vivo* detection, patient PBMCs were recalled with 2 mM peptide or DMSO for 6 or 24h. For patient PBMCs pre-exposed to neoantigen peptide, CD3 $^-$ APCs were isolated from fresh PBMCs using CD3 microbeads (Miltenyi) and co-cultured with CD3 $^+$ T cells at a T cell:APC ratio of 2:1 and recalled with 2mM peptide or DMSO for 6 or 24h. Anti-CD107a antibody was added 6h prior to the end of co-culture. GolgiStop/Plug (BD Biosciences) were added 4h prior to the end of co-culture. Subsequently, cells were stained with cell surface antibodies at 4 °C for 30 min, followed by fixation/permeabilization with Fixation and Permeabilization

Solution (BD Biosciences), and subsequently stained with antibodies against intracellular proteins at 4 °C for 30 min. Cells were stored in FACS buffer at 4 °C until acquisition on a BD LSR Fortessa instrument. Gating was performed for IFN γ and CD107a based on FMO stained controls.

MHCII protein expression, purification, and peptide exchange

Signal peptides and ectodomains of alpha and beta MHC class II alleles were encoded as fusions to heterodimeric coiled coils in a pcDNA3.4 vector (Thermo Fisher Scientific). Allele-specific placeholder epitope peptides were covalently fused to the N-terminus of each beta allele. Soluble heterodimers of alpha/beta proteins were secreted directly into culture media post-transfection into Expi293F cells (Thermo Fisher Scientific) and purified using HisTrap Excel media (Cytiva). Purified MHC class II alleles were subsequently biotinylated and the placeholder peptide cleaved prior to peptide exchange. Epitope peptides (at 20-fold molar excess to allele) were loaded onto purified MHC II alleles using equimolar recombinant soluble HLA-DM overnight at 37°C.

Multimer generation and staining

Dual-multimer approach was used where each peptide-HLA II allele was conjugated to two different streptavidin fluorophores. Peptide exchanged allele was incubated with fluorochrome-conjugated streptavidin antibodies on ice for 30 min in the dark. Biotin was added to block any unoccupied sites on streptavidin fluorophore. Reaction was spun down at 3500 RPM (4°C) for 10 min to remove any aggregates. The conjugated multimer supernatants were used for making a pooled multimer mix.

Patient PBMCs were thawed and subjected to T cell enrichment by using a human Pan T Cell Isolation Kit (Miltenyi Biotech). Isolated T cells were counted and treated with Benzonase and 50nM Dasatinib for 20 min at 37°C in RPMI media containing 10% FBS. Enriched T cells were centrifuged at 1500 RPM for 5 min, washed once with FACS buffer (1X PBS +0.5% BSA) supplemented with 50nM dasatinib, and plated in a 96-well plate (3x106 cells/well). Cells were resuspended in a pooled multimer mix made in FACS buffer and incubated for 1 h at 37°C.

Phenotyping of multimer⁺ CD4⁺ T cells

Phenotyping of neoantigen-specific CD4⁺ T cells was performed as described previously (Ott et al., 2020). PBMCs were thawed and treated with 0.025 U/ml benzonase and 50 nM dasatinib in X-Vivo media (Lonza) at 37°C for 20 min. Cells were then stained with MHC Class II tetramers at 37°C for 1 h, followed by staining with surface antibodies at 4°C for 30 min. Cells were fixed at 20°C for 20 min using the Fixation/Permeabilization Kit (BD Biosciences). Cells were washed and stored in FACS buffer at 4°C until acquisition on a BD LSR Fortessa instrument.

RNA extraction from FFPE tumors and PBMCs

For FFPE tumor blocks, 2–4 scrolls of 20 mM thickness were deparaffinized using heptane and RNA was extracted using the AllPrep DNA/RNA FFPE kit according to the manufacturers' instructions (QIAGEN). PBMCs were thawed and subjected to negative selection using the Pan T cell Isolation Kit (Miltenyi) according to manufacturer's protocol. T cells were counted, centrifuged for 15 min at 300xg then flash frozen and stored as dry pellets at –80°C. RNA isolation was performed using the RNeasy Plus Micro Kit (QIAGEN) on the QIAcube (QIAGEN; Protocol: Purification of total RNA using gDNA Eliminator and RNeasy MinElute spin columns) according to manufacturer's protocol. RNA concentration was measured using the Qubit RNA HS Assay Kit (ThermoFischer) according to manufacturer's protocol. Eluted RNA was stored at –80°C.

Gene expression analysis

Using the transcript per million (TPM) quantification of gene expression from the tumor biopsy RNA, we summed the TPM values for all detected HLA-DR, HLA-DP and HLA-DQ per patient. The log-transformed values were plotted against each patient PFS.

TCR library preparation and sequencing

TCR β libraries were prepared from isolated RNA using the Long Read iR-Profile Reagent System (iRepertoire) at the iRepertoire headquarters according to manufacturer's protocol. Libraries were sequenced using the MiSeq Reagent Kit v2 300-cycles (Illumina) at the iRepertoire headquarters according to manufacturer's protocol. Throughout the study, the number of samples per pool was designed to maintain equal sequencing depths across samples.

TCR repertoire generation

TCR repertoires were generated by running a licensed copy of MiXCR 3.0.12 on the paired-end raw sequencing fastq files. The parameters included the species specifications (Human, hsa), starting material (RNA), 5 and -3' primers (v and c primers, respectively) with no adapters, and searching for either TCR α (tra) or TCR β chains (trb). TCR α or TCR β CDR3 clonotypes were filtered by removal of non-functional sequences (out-of-frame sequences or those containing stop codons). Clonal frequency was calculated based on the count for each clone out of the total count.

TCR repertoire diversity/clonality analysis

The unique number of nucleotide/amino acid TCR α or TCR β CDR3s was calculated per sample. Global diversity/clonality coefficients have been calculated as follows:

Gini Coefficient – ranges between 0 (all clones are equally frequent – repertoire diversity) and 1 (frequency dominated by one clone, repertoire clonality). Calculated using the “Gini” function from the “DescTools” R package (Signorell et al., 2016).

Normalized Shannon’s Entropy – higher values represent higher inequality of the frequencies (Jia et al., 2015; Hanson et al., 2020).

Single-cell RNA sequencing of neoantigen-specific CD4⁺ T cells using HLA class II multimer staining

Cell surface protein labeling for single-cell RNA sequencing and cell sorting

After HLA Class II multimer staining, Fc blocking was performed through incubation with human FcR Blocking Reagent (Miltenyi Biotech) for 10 min at 4 °C. For cell surface protein labeling for sequencing, a mix of 19 TotalSeq-C antibodies (BioLegend) was added to the multimer-stained cells. Cells were simultaneously labeled with FITC anti-human CD4 (BD), BV711 anti-human CD3 (BD), AF700 anti-human CD8 (BioLegend) antibodies, and LIVE/DEAD Fixable Near-IR Dead Cell Stain Kit (Thermo Fisher). After 30-min of incubation at 4°C, cells were washed twice in PBS with 1% BSA and sorted using a BD Aria cell sorter (BD Bioscience). For each patient sample, two different CD4⁺ T cell populations were sorted: Tetramer⁻ CD4⁺ (Live CD3⁺ CD4⁺ CD8⁻) and Tetramer⁺ CD4⁺ (Live CD3⁺ CD4⁺ CD8⁻ ASP multimer⁺).

Single-cell TCR, surface epitope and transcriptome sequencing

After sorting, labeled cells were resuspended at ~1x10³ cells/ml in PBS supplemented with 2% FBS and submitted to subsequent single-cell RNA sequencing (scRNA-Seq) processes. Sample processing for single-cell gene expression (GEX), TCR V(D)J clonotypes (VDJ), and cell surface protein expression (CITE) libraries was performed following the manufacturer’s protocol (Chromium Next GEM Single Cell 5’ Reagent Kits v2 (Dual Index), 10X Genomics). Briefly, sorted Tetramer⁺ and Tetramer⁻ CD4⁺ T cell suspensions were partitioned into nanoliter-scale Gel Beads-in-Emulsions (GEMs) using a Chromium Controller (10X Genomics). Subsequent Gel Bead-in-Emulsion reverse transcription (GEM-RT) reaction & post clean-up and cDNA amplification were carried out to generate cDNAs for scRNA-Seq libraries. Constructing cDNA libraries for GEX (Library Construction Kit), VDJ (Chromium Single Cell Human TCR Amplification Kit) and CITE (5’ Feature Barcode kit) was performed based on the manufacturer’s protocols. All sequencing library quality controls were performed by using Bioanalyzer High Sensitivity DNA Chip Kits with an Agilent 2100 Bioanalyzer (Agilent Technology). Sequencing libraries were quantified using KAPA Library Quantification Kits - Complete kit and LightCycler 480 (Roche).

All libraries were incorporated with Sample Index sequences (Dual Index Kit TN Set A for CITE libraries and Dual Index Kit TT Set A for VDJ & GEX libraries) and sequenced on MiSeq (MiSeq Reagent Kit v2 (300-cycles)) or NovaSeq S1 platform (Illumina) depending on sequencing depth. The sequencing parameters were: Read 1 of 26 cycles, i7 Index of 10 cycles, i5 Index of 10 cycles, and Read 2 of 90 cycles.

Single-cell RNA sequencing data analysis

Cell Ranger version 6.0.1 (10X Genomics) was used to align raw sequencing data with “count” option. Library with RNA was aligned on GRCh38-2020-A genome. TCR library was aligned on vdj_GRCh38_alts_ensembl-5.0.0 assembly. CITE library was aligned on a custom panel of antibodies. R package Seurat 4.0.4 (Stuart et al., 2019) was used for downstream analysis of data acquired from cellranger count. We filtered cells that (1) had more than 25% of mitochondrial gene content, (2) had less than 1024 UMI from RNA or 3) had less than 90 UMI for CITE library. RNA library was log-normalized with a scale factor of 10⁴. The 2000 most variable genes were detected by the FindVariableFeatures function. These 2000 genes were overlaid with 10X Genomics Immunological panel (1056 genes) to de-noise the list, resulting in 344 genes used in downstream analysis. Latent variables - number of UMI’s and mitochondrial content - were regressed out using a negative binomial model with function ScaleData. Principal component analysis (PCA) was performed with the RunPCA function. For RNA library harmony function was called (R package Harmony, (Korsunsky et al., 2019)) to remove donor effect. CITE library was normalized using CLR method, scaled (by ScaleData function) using all available antibodies (except for LAG3, TIM3, 41BB, CTLA4 and KLIG1 that had low expression and off-target binding) and PCA was run on it. RNA- and CITE-processed data were used to run WNN method by FindMultiModalNeighbors function to create new modality to run dimensionality reduction and clustering that takes into account RNA and protein levels. A UMAP dimensionality reduction was performed on the WNN using the first 20 PCA components for harmonized RNA and 13 for CITE to obtain a two-dimensional representation of the cell states. For clustering, we used and FindClusters function with SLM algorithm and resolution 0.25. To identify marker genes, we used FindAllMarkers function to compare cluster against all other clusters, and FindMarkers to compare selected clusters. For each cluster, only genes that were expressed in more than 15% of cells with at least 0.15-fold differences were considered. For heatmap representation we used mean expression of protein markers inside each cluster. Heatmaps were built with ComplexHeatmap R package (Gu et al. 2016). To analyze TCR we filtered out all TCR that did not correspond to cell barcode in RNA + CITE library post quality control. Gini coefficient was computed with DescTools R package.

Cloning of neoantigen-specific TCRs

Lentivirus vectors were generated on 293FT producer cell lines using shuttle plasmids (GenScript) containing TCR beta and alpha chains under the control of an SFFV promoter and separated by a furin cleavage site and a P2A ribosomal skip sequence. Human TCR variable regions were fused to cysteine-modified mouse constant regions for both chains resulting in recombinant mTCR (Cohen et al., 2006; Kuball et al., 2007). The mTCR-transduced, puromycin-selected (Thermo Fisher) Jurkat cells were expanded in RPMI media supplemented with 10% FBS (Thermo Fisher). Neoantigen reactivity of the mTCR Jurkat cells was determined by IL-2 secretion measured by electrochemiluminescence (MSD) in 24-h *in vitro* assays where mTCR transduced Jurkat cells were co-cultured with neoantigen peptide and CD3⁺ T cell-depleted autologous patient PBMCs.

MultiOmyx staining

For multiplexed T cell analysis, multiplexing immunofluorescence (IF) analysis on FFPE tumor blocks was performed at NeoGeonomics Laboratories (Lake Forest, CA). Each FFPE slide was presented to a NeoGenomics pathologist for tissue annotation and selection. The areas selected to be tumor-relevant by the pathologist were used for staining and analysis. The staining was performed using a single 4 μ M FFPE slide. Slides were prepared and stained using MultiOmyx optimized protocols by Neogeneomics. For each round of staining, conjugated fluorescent antibodies are applied to each slide, followed by image acquisition of stained slides. The dye is then quenched allowing for subsequent rounds of staining with other antibodies. Proprietary deep learning-based workflows were applied to identify individual cells and perform cell classification for all individual markers, as well as to identify tissue and tumor regions for analysis. Individual cell and region classification results were combined to generate co-expression summaries for phenotypes of interest. Antibodies used for staining include CD3, CD4, CD8, Pan CK, DAPI. Analysis was performed according to NeoGeonomics Laboratories' optimized protocols ([Gerdes et al., 2013](#); [Xu-Monette et al., 2019](#)).

Multiplex IHC staining protocol

Multiplex immunofluorescence (mIF) staining was performed on 4 μ m FFPE tumor sections using the OPAL mIHC kit (Akoya Biosciences). Briefly, sections were deparaffinized and rehydrated. Antigen retrieval was performed in a using an antigen unmasking solution (citrate-based and tris-based). Protein blocking was performed for 10 min using Antibody Diluent/Block solution (Akoya Biosciences). Primary antibodies were incubated for 30 min at RT. Slides were then incubated with Polymer-HRP(Vector Labs) diluted 1:1 with TBS for 30 min. For visualization with OPAL fluors, slides were incubated for 10 min with OPAL colors. Another heat step consisting of boiling the slides in antigen unmasking solution was performed to remove the antibody complexes. The same sequence of blocking, primary antibody incubation, Polymer-HRP application and heating was repeated for each antibody in the multiplex sequence. Finally, the slides were counterstained with DAPI, mounted with prolong gold and coverslipped. Some antibodies used in staining panels include CD3, CD4, HLA DP/DQ/DR, and Pan Ck.

Multispectral analysis

The multiplex slides were scanned with a Vectra 3.0 microscope system (Perkin Elmer). Whole slide scans were performed using the 10 \times objective lens. Up to ten individual fields were selected in the Phenochart program (Phenochart 1.0.9, Perkin Elmer) for higher resolution scanning at 20 \times (669 \times 500 μ m). Multispectral images were unmixed and analyzed using inForm software (inForm 2.4.2, Perkin Elmer) and analyzed with tissue component segmentation based on tumor cell staining: tumor = Pan Ck + regions and stroma = Pan Ck-regions. Individual cells (defined by DAPI positive nuclei) were then phenotyped to characterize various cell populations. Density of cells in each ROI was calculated by combining the cell counts from all images and normalizing by the total area (cells/mm²).

Statistical analysis

Statistical analyses of clinical data were performed using SAS (version 9.2). All other analyses were performed in either the R language and environment for statistical computing (version 4.0.0) or GraphPad Prism (version 7.01). Likewise, all figures were created using an R script on the “ggplot2” package ([Wickham 2016](#)) or GraphPad Prism. Unless otherwise specified, p values were derived from a two-tailed Student's *t* test.

ADDITIONAL RESOURCES

All data presented in this manuscript is from the multicenter phase I clinical trial NCT03380871. The study's protocol is provided in [Data S1](#).